Research Article

Investigation of Free Vibration in Fluid-Loaded Cylindrical Shells with a Three-Layer Sandwich Wall and an Auxetic Central Layer

Korosh Khorshidi *[ID], Saboor Savvafi, Sadegh Zobeid

Department of Mechanical Engineering, Faculty of Engineering, Arak University, Arak, 38156-88349, Iran

ARTICLE INFO

ABSTRACT

Using novel materials, including auxetic structures, has witnessed significant growth. Consequently, a comprehensive examination of their mechanical behavior becomes imperative. This study delves into the free vibration characteristics of a three-layer cylindrical shell containing liquid. The central layer of this structure features a re-entrant honeycomb auxetic pattern, while the inner and outer layers are assumed to be isotropic and constructed from aluminum. The liquid within the shell is considered ideal and incompressible, with no consideration for wave effects on its free surface. To model this problem, we employ a modified high-order shear deformation theory (HSDT). By applying Hamilton's principle, we derive fundamental equations and solve them using the Galerkin weighted residual method. We compare our findings with results published in authoritative articles and outcomes obtained from finite element analysis in ABAQUS to validate them. Our investigation explores the impact of various parameters on the natural frequencies of the cylindrical body. These parameters include the geometrical dimensions of the sandwich cylindrical cover, adjustable auxetic core parameters, and liquid characteristics. Given the widespread use of cylindrical sandwich shells across diverse industries, our study provides valuable insights into the phenomenon of free vibration in these structures. Remarkably, previous studies have not investigated the free vibration of a three-layered cylindrical shell with an auxetic structure and liquid interaction.

1. Introduction

Poisson's ratio is a well-known measure used to describe material behavior during tension and compression. Due to their cellular networks, auxetic structures are categorized as materials with a negative Poisson ratio (NPR). These materials expand and contract in the axial direction due to stretching and compression.

In our current world, one of the primary goals of research on smart structures is to achieve materials or designs capable of absorbing high energy during events involving heavy loads. Conversely, developing a material that can absorb substantial energy while remaining lightweight presents a significant challenge. Various auxetic structures offer a solution to achieving these goals. Compared to similar conventional samples, auxetic structures exhibit superior mechanical properties. Properties such as higher load-bearing capacity and stiffness, higher shear modulus, improved hardness and resistance to fracture, high damping coefficient in vibration absorption, and excellent ability to

---

* Corresponding author.
E-mail address: *k-khorshidi@araku.ac.ir*
Tel.: +98 863 262 5720
Fax: +98 863 417 3450

Cite this article as:

absorb energy are among these properties[1, 2]. Due to the unique behavior and high energy absorption capacity, using auxetic structures as a core in sandwich panels is interesting (see Refs. [3, 4]). In order to understand the principal equations for exploring vibration in auxetic structures, we studied literature about sandwich plates and shells composed of auxetic cells. Salehi et al.[5] investigated damping effects on the vibration behavior of a sandwich cylindrical sell. Equations of motion are derived using transverse modal coordinates in the frequency domain. The assumed-mode method is employed to solve these equations. Thickness effects of constrained and viscoelastic layers are explored through transient external load responses, focusing on damping factors and settling times. Ranjbar et al.[6] investigated the oscillation of sandwich panels with an anti-tetrachiral auxetic core. By utilizing the finite element method, they obtained the mechanical properties of the auxetic body and the natural frequencies of the system, and it determined that both structures have a good effect on the structure's vibration behavior and natural frequencies. Mazloomi et al.[7] proposed a new 2D-scaled structure with anti-tetrachiral cells. In this study, they evaluated the numerical response of the vibrations of sandwich panels with an auxetic core. They performed a modal analysis of the structure using a homogenized finite element model. The authors obtained the optimal structures for the core. Hosseinkhani et al.[8] studied the acoustic vibration behavior of sandwich panels with an anti-tetrachiral structure containing a resonator. The authors showed that using local regenerators in anti-tetrachiral structures can significantly reduce the noise of panels, especially under local loading conditions. This study provides valuable insights into the acoustic vibration behavior of sandwich panels with an anti-tetrachiral structure. Hosseinkhani et al.[9] investigated the vibration and acoustic behavior of sandwich panels with an anti-tetrachiral structure containing a resonator. Their study demonstrated that incorporating local resonators in anti-tetrachiral structures can significantly reduce panel noise, particularly under local loading conditions. Mazloomi et al.[10] managed a study on the vibration of sandwich panels with a core of hexagonal structure inside the auxetic face. Using an auxetic core allows us to adjust the local mechanical properties of the sandwich structure in different areas of the panel. The authors obtained the natural frequency of the structure and the radiated sound power level of the sandwich panel using the homogeneous finite element model. They compared it with the full-scale model of the structure. The obtained results show a good agreement between the results of both models.

Pakrooyan et al.[11] investigated the free vibration of a sandwich plate with an auxetic core as the wall of the fluid tank. The re-internal honeycomb auxetic structure was used. They concluded that increasing the thickness of the auxetic sheet results in an increase in the natural frequency and a decrease in the cell aspect ratio. Khorshidi et al. [12] studied energy harvesting using a sandwich panel made with an auxetic core and layers of piezoelectric materials. The study investigated the impact of various parameters, such as the auxetic cell's geometry and carbon nanotubes' volume and their configuration, on electric power and voltage. In this particular system, structures exhibiting negative Poisson ratios demonstrated significantly superior energy harvesting efficiency compared to traditional structures. The research also revealed that incorporating auxetic materials into piezoelectric systems increases efficiency, thanks to their remarkable properties. Duke et al.[13] carried out a study on the nonlinear dynamic response and vibration of composite cylindrical panels on an elastic bed. The study investigated the effects of panel geometrical parameters, blast load, and damping on natural frequencies. The authors found that the natural frequencies of the panels were affected by the geometrical parameters, blast load, and damping. Fu et al.[14] managed a study on the energy absorption properties of the auxetic structure by investigating a three-layer curved shell with an auxetic core and tops made of FGM materials under an impact force. The study investigated the effect of parameters such as volume ratio, radius of curvature, porosity ratio, and cell structure geometry on impact energy absorption. Karimiasl and Alibiglou [15] studied the free and forced vibration under harmonic load for a three-layered cylindrical shell with graphene layers and an auxetic core. They studied a double V-shaped honeycomb in a thermal and humid environment.

This study investigates the free vibration of a three-layer cylindrical shell containing liquid. The central layer of the body has a re-internal honeycomb auxetic structure, and the inner and outer layers are assumed to be isotropic (aluminum). The liquid is considered incompressible and ideal, and the effects of waves on the free liquid's surface are ignored. The problem was modeled physically using Modified high-order shear deformation theory (HSDT). The fundamental equations were derived by applying Hamilton's principle and resolved by the Galerkin weighted residual solution. The results of this investigation have been compared and confirmed with the results published in authoritative articles and the outcomes derived from finite element analysis in ABAQUS. The

effect of various parameters, such as geometrical dimensions of the sandwich cylindrical cover, adjustable parameters of the auxetic core, and liquid characteristics on the natural frequencies of the cylindrical body, have been investigated. It is worth noting that previous studies have not addressed sandwich cylinders with an auxetic structure while considering the fluid's impact on their behavior.

In this study, we also delve into a more detailed investigation of the mentioned behavior by incorporating exponential, trigonometric, hyperbolic, and parabolic functions within the theory of high-order shear deformation (HSDT). The present article serves as a valuable resource for the detailed presentation of mathematical relationships related to the exact solution of the vibration behavior of cylindrical sandwich shells. Notably, all the expansions of relations presented in this article are provided in expanded form for the first time.

2. Define the Problem

This research aims to obtain the equation governing the free vibration of a three-layered cylindrical shell with length L, radius R, and total thickness h containing an incompressible liquid at height H, as shown in Fig.1. The cylindrical coordinate system is considered for coordination and convenience.

3. Mathematical Modeling

3.1 Cylindrical Shell

It has been proven that for modified shear deformation theory, the rotational inertias σxz and the distribution of shear stresses σθz assumed to be non-zero, and in the free surfaces (tops), the said shear stresses are zero, and these theories do not require a shear correction factor. Consequently, the displacement field for cylindrical shells is considered as Eq. (1).[16]

$$u_1(x, \theta, z, t) = u_0(x, \theta, t) - f_1(z) + \frac{\partial w(x, \theta, t)}{\partial x} f_2(z)\varphi_1(x, \theta, t) \quad \text{(1-a)}$$

$$u_2(x, \theta, z, t) = v_0(x, \theta, t) - \frac{f_1(z)}{R}\left(\frac{\partial w(x, \theta, t)}{\partial \theta} - v(x, \theta, t)\right) + f_2(z)\varphi_2(x, \theta, t) \quad \text{(1-b)}$$

$$u_3(x, \theta, z, t) = w_0(x, \theta, t) \quad \text{(1-c)}$$

where Eq. (1), $u_0(x, \theta, t)$, $v_0(x, \theta, t)$, $w_0(x, \theta, t)$, represent the cylindrical shell's longitudinal

displacement, circumferential displacement, and transverse displacement, respectively. $\varphi_1(x, \theta, t)$ and $\varphi_2(x, \theta, t)$ represent the rotation of the middle plane around the θ and x axes, respectively. $f_2(z)$ and $f_1(z)$ are also considered for different theories, as shown in Table 1[17]. Assuming the linearity of the strain-displacement relations for the cylindrical shell, it will be in the form of Eq. (2) [18].

$$\varepsilon_{xx} = \frac{\partial u_1}{\partial x} = \frac{\partial u_0}{\partial x} + f_1(z)\frac{\partial^2 w_0}{\partial x^2} + f_2(z)\frac{\partial \phi_1}{\partial x} \quad \text{(2-a)}$$

$$\begin{aligned}\varepsilon_{\theta\theta} &= \frac{1}{R}\left(\frac{\partial u_2}{\partial x} + u_3\right) \\ &= \frac{1}{R}\left(w_0 + \frac{\partial v_0}{\partial \theta}\right) \\ &+ \frac{f_1(z)}{R^2}\left(\frac{\partial^2 w_0}{\partial \theta^2} - \frac{\partial v_0}{\partial \theta}\right) \\ &+ \frac{f_2(z)}{R}\frac{\partial \phi_2}{\partial \theta}\end{aligned} \quad \text{(2-b)}$$

$$\begin{aligned}\gamma_{x\theta} &= \frac{1}{R}\frac{\partial u_1}{\partial \theta} + \frac{\partial u_2}{\partial x} \\ &= \frac{\partial v_0}{\partial x} \\ &+ \frac{f_1(z)}{R}\left(\frac{\partial^2 w_0}{\partial x\partial \theta} - \frac{\partial v_0}{\partial x}\right) \\ &+ \frac{1}{R}\left(\frac{\partial u_0}{\partial \theta} + f_1(z)\frac{\partial^2 w_0}{\partial x\partial \theta}\right) \\ &+ f_2(z)\frac{\partial \phi_1}{\partial \theta}\right) + f_2(z)\frac{\partial \phi_2}{\partial x}\end{aligned} \quad \text{(2-c)}$$

$$\begin{aligned}\gamma_{xz} &= \frac{\partial u_3}{\partial x} + \frac{\partial u_1}{\partial z} = \frac{\partial w_0}{\partial x}\left(1 + \frac{\partial f_1(z)}{\partial z}\right) \\ &+ \frac{\partial f_2(z)}{\partial z}\phi_1\end{aligned} \quad \text{(2-d)}$$

$$\begin{aligned}\gamma_{\theta z} &= \frac{1}{R}\frac{\partial u_3}{\partial \theta} + \frac{\partial u_2}{\partial z} - \frac{u_2}{R} \\ &= \left(1 + \frac{\partial f_1(z)}{\partial z}\right)\left(\frac{1}{R}\frac{\partial w_0}{\partial \theta}\right) \\ &- \frac{v_0}{R}\right) + \frac{\partial f_2(z)}{\partial z}\phi_2\end{aligned} \quad \text{(2-e)}$$

Table 1: Mathematical Theories for Modeling Configurations[17]

Theory	$f_1(z)$	$f_2(z)$
ESDPT	$-z$	$ze^{-2\left(\frac{z}{h}\right)^2}$
TSDPT	$-z$	$\frac{h}{\pi}\sin\left(\frac{\pi z}{h}\right)$
HSDPT	$-z$	$h\sinh\left(\frac{z}{h}\right) - z\cosh\left(\frac{1}{2}\right)$
PSDPT	$-z$	$z\left(\frac{5}{4} - \frac{5}{3h^2}z^2\right)$

The cylindrical shell comprises three layers, with the middle layer (core) having an auxetic structure. The inner and outer layers are assumed to be isotropic. As a result, the stress-strain relations are expressed in the form of Eq. (3)[12] .
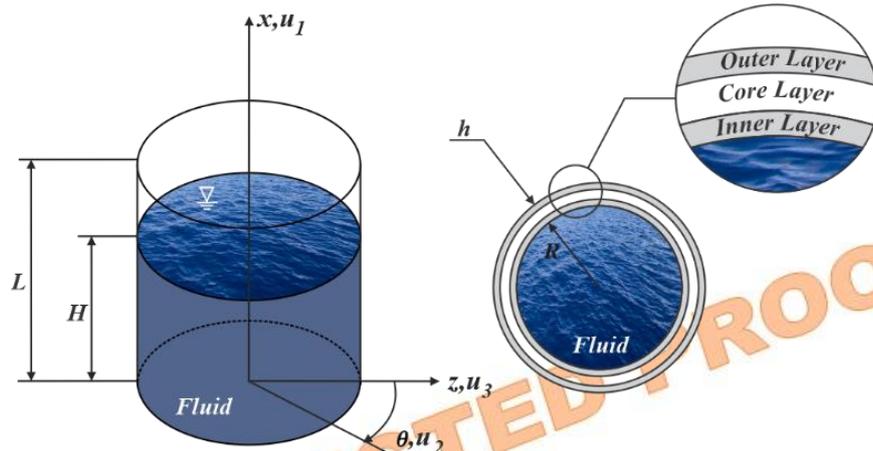
Fig. 1: A Cylindrical Shell Containing Fluid with Assumed Coordinates Is the Subject of This Study.

$$\begin{Bmatrix} \sigma_{xx} \\ \sigma_{\theta\theta} \\ \sigma_{\theta z} \\ \sigma_{xz} \\ \sigma_{x\theta} \end{Bmatrix} = \begin{bmatrix} Q_{11}^{(k)} & Q_{12}^{(k)} & 0 & 0 & 0 \\ Q_{21}^{(k)} & Q_{22}^{(k)} & 0 & 0 & 0 \\ 0 & 0 & Q_{44}^{(k)} & 0 & 0 \\ 0 & 0 & 0 & Q_{55}^{(k)} & 0 \\ 0 & 0 & 0 & 0 & Q_{66}^{(k)} \end{bmatrix} \cdot \begin{Bmatrix} \varepsilon_{xx} \\ \varepsilon_{\theta\theta} \\ \gamma_{\theta z} \\ \gamma_{xz} \\ \gamma_{x\theta} \end{Bmatrix}, k = 1,2,3 \quad (3)$$

where:

$$Q_{11}^{(k)} = \frac{E_1^{(k)}}{1 - v_{12}^{(k)} v_{21}^{(k)}} \quad (4\text{-a})$$

$$Q_{12}^{(k)} = \frac{E_2^{(k)} v_{12}^{(k)}}{1 - v_{12}^{(k)} v_{21}^{(k)}} \quad (4\text{-b})$$

$$Q_{22}^{(k)} = \frac{E_2^{(k)}}{1 - v_{12}^{(k)} v_{21}^{(k)}} \quad (4\text{-c})$$

$$Q_{44}^{(k)} = G_{23}^{(k)}, Q_{55}^{(k)} = G_{13}^{(k)}, Q_{66}^{(k)} = G_{12}^{(k)} \quad (4\text{-d})$$

Equation (4) defines the shear modulus, Young's modulus, and Poisson's ratio of the outer and core layers as $v_{21}^{(k)}, v_{12}^{(k)}, G_{23}^{(k)}, G_{12}^{(k)}, G_{13}^{(k)}, E_2^{(k)}$, and $E_1^{(k)}$. In Eq. (3), $k = 3,1$ represents the outer and inner layers of isotropic materials. In this research, $k = 2$ represents the auxetic core, which is the structure and coordinates of the unit cell inside the auxetic surface, according to Figure 2 [19]. The elastic parameters of the auxetic layer are calculated using Eq. (5), which include the tensile and bending deformations of the cells.

$$E_1^{(2)} = E_s \frac{(\eta_3 \sec \theta_1)^3 (\eta_1 + \sin \theta_1)}{[1 + \eta_3^2 (\tan^2 \theta_1 + \eta_1 \eta_2 \sec^2 \theta_1)]} \quad (5\text{-a})$$

$$E_2^{(2)} = E_s \frac{\eta_3^3 \sec \theta_1}{(\eta_1 + \sin \theta_1)(\tan^2 \theta_1 + \eta_3^2)} \quad (5\text{-b})$$

$$G_{12}^{(2)} = E_s \frac{\eta_3^3 \sec \theta_1 (\eta_1 + \sin \theta_1)}{\eta_1^2 (1 + 2\eta_1 \eta_2^3)} \quad (5\text{-c})$$

$$G_{23}^{(2)} = G_s \frac{\eta_3 \cos \theta_1}{\eta_1 + \sin \theta_1} \quad (5\text{-d})$$

$$G_{31}^{(2)} = G_s \frac{\eta_3 \sec \theta_1}{2\eta_2 (\eta_1 + \sin \theta_1)(\eta_1 + 2\eta_2)} \quad (5\text{-e})$$

$$v_{12}^{(2)} = \frac{\sec \theta_1 \tan \theta_1 (1 - \eta_3^2)(\eta_1 + \sin \theta_1)}{[1 + (\tan^2 \theta_1 + \eta_1 \eta_2 \sec^2 \theta_1) \eta_3^2]} \quad (5\text{-f})$$

$$v_{21}^{(2)} = \frac{\sin \theta_1 (1 - \eta_3^3)}{(\tan^2 \theta_1 + \eta_3^2)(\eta_1 + \sin \theta_1)} \quad (5\text{-g})$$

$$\rho^{(2)} = \rho_s \frac{\eta_3 (\eta_1 + 2)}{2 \cos \theta_1 (\eta_1 + \sin \theta_1)} \quad (5\text{-h})$$

where $\eta_2 = \frac{t_2}{t_1}, \eta_3 = \frac{t_1}{l_1}$ and $\eta_1 = \frac{l_2}{l_1}$. Also, G_s and E_s are the elastic layer properties, and ρ_s is the density of the base material of the auxetic core. Additionally, isotropic layers with $k = 3,1$, Eq. (4) was obtained as Eq. (6) [12].

$$Q_{11}^{(1,3)} = Q_{22}^{(1,3)} = \frac{E}{1 - v^2} \quad (6\text{-a})$$

$$Q_{12}^{(1,3)} = Q_{21}^{(1,3)} = \frac{v E}{1 - v^2} \quad (6\text{-b})$$

$$Q_{44}^{(1,3)} = Q_{55}^{(1,3)} = Q_{66}^{(1,3)} = G = \frac{E}{2(1 + v)} \quad (6\text{-c})$$

Equation (6) relates the shear modulus, Young's modulus, and Poisson's ratio of the inner and outer layers to E, G, v, respectively. Hamilton's principle, which is utilized to derive the equations governing the motion, is consistent with Eq. (7)[20].

$$\int_0^t \delta(T - U)dt = 0 \quad (7)$$

where δ defines the variation of function, and T and U are the system's strain energy and kinetic energy, respectively.
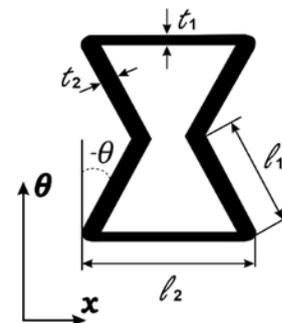

Fig.2. An internal Honeycomb Cell Structure[19] .

4

3.2 Strain Energy

Equation (8) used to obtain the strain energy of the three-layer cylindrical shell [11].

$$U = \frac{1}{2}\sum_{k=1}^{3}\int_{\forall^{(k)}}\left(\{\sigma_{xx}, \sigma_{\theta\theta}, \sigma_{x\theta}, \sigma_{xz}, \sigma_{\theta z}\}^{(k)} \cdot \{\varepsilon_{xx}, \varepsilon_{\theta\theta}, \gamma_{x\theta}, \gamma_{xz}, \gamma_{\theta z}\}\right)d\forall^{(k)} \quad (8)$$

Also, strain energy changes obtained in the form of Eq. (9) [11]

$$\delta U = \int_{A}\int_{\frac{-h}{2}}^{\frac{h}{2}}(\sigma_{xx}\delta\varepsilon_{xx} + \sigma_{\theta\theta}\delta\varepsilon_{\theta\theta} + \sigma_{x\theta}\delta\gamma_{x\theta} + \sigma_{xz}\delta\gamma_{xz} + \sigma_{\theta z}\delta\gamma_{\theta z})dzdA \quad (9)$$

By substituting the equations of Eq. (2) into Eq. (9) and partial integration, the strain energy changes can be expressed as Eq.(10):

$$\delta U = \int_{A}\left(\left(-\frac{\partial N_{xx}}{\partial x}\delta u_0 + \frac{\partial^2 S_{xx}}{\partial x^2}\delta w_0\right.\right.$$
$$-\frac{\partial P_{xx}}{\partial x}\delta\phi_1 - \frac{1}{R}\frac{\partial N_{\theta\theta}}{\partial\theta}\delta v_0$$
$$+\frac{1}{R^2}\frac{\partial^2 S_{\theta\theta}}{\partial\theta^2}\delta w_0$$
$$+\frac{1}{R^2}\frac{\partial S_{\theta\theta}}{\partial\theta}\delta v_0$$
$$-\frac{1}{R}\frac{\partial P_{\theta\theta}}{\partial\theta}\delta\phi_2 + \frac{N_{\theta\theta}}{R}\delta w_0$$
$$-\frac{\partial N_{x\theta}}{\partial x}\delta v_0 + \frac{2}{R}\frac{\partial^2 S_{x\theta}}{\partial x\partial\theta}\delta w_0 \quad (10)$$
$$+\frac{1}{R}\frac{\partial S_{x\theta}}{\partial x}\delta v_0 - \frac{\partial P_{x\theta}}{\partial x}\delta\phi_2$$
$$-\frac{1}{R}\frac{\partial N_{x\theta}}{\partial\theta}\delta u_0$$
$$-\frac{1}{R}\frac{\partial P_{x\theta}}{\partial\theta}\delta\phi_1 - \frac{\partial T_{xz}}{\partial x}\delta w_0$$
$$+Q_{xz}\delta\phi_1 - \frac{1}{R}\frac{\partial T_{\theta z}}{\partial\theta}\delta w_0$$
$$\left.\left.-\frac{T_{\theta z}}{R}\delta v_0 + Q_{\theta z}\delta\phi_2\right)dA\right.$$

where:

$$\{P_{xx}, P_{\theta\theta}, P_{x\theta}\} = \sum_{k=1}^{3}\int_{z_{k-1}}^{z_k}\{\sigma_{xx}, \sigma_{\theta\theta}, \sigma_{x\theta}\}^{(k)}f_2(z)\,dz \quad (11\text{-a})$$

$$\{N_{xx}, N_{\theta\theta}, N_{x\theta}\} = \sum_{k=1}^{3}\int_{z_{k-1}}^{z_k}\{\sigma_{xx}, \sigma_{\theta\theta}, \sigma_{x\theta}\}^{(k)}dz \quad (11\text{-b})$$

$$\{S_{xx}, S_{\theta\theta}, S_{x\theta}\} = \sum_{k=1}^{3}\int_{z_{k-1}}^{z_k}\{\sigma_{xx}, \sigma_{\theta\theta}, \sigma_{x\theta}\}^{(k)}f_1(z)\,dz \quad (11\text{-c})$$

$$\{Q_{xz}, Q_{\theta z}\} = \sum_{k=1}^{3}\int_{z_{k-1}}^{z_k}\{\sigma_{xz}, \sigma_{\theta z}\}^{(k)}\frac{\partial f_2(z)}{\partial z}\,dz \quad (11\text{-d})$$

$$\{T_{xz}, T_{\theta z}\} \quad (11\text{-e})$$

$$= \sum_{k=1}^{3}\int_{z_{k-1}}^{z_k}\{\sigma_{xz}, \sigma_{\theta z}\}^{(k)}\left(\frac{\partial f_1(z)}{\partial z} + 1\right)dz$$

3.3 Kinetic Energy:

Equation (12) is used to obtain the kinetic energy [11].

$$T = \frac{1}{2}\sum_{k=1}^{3}\rho^{(k)}\int_{\forall^{(k)}}(\dot{u}_1^2 + \dot{u}_2^2 + \dot{u}_3^2)d\forall^{(k)} \quad (12)$$

Equation (13) describes the changes in the system's kinetic energy [11] :

$$\delta T = \int_{A}\int_{-\frac{h}{2}}^{+\frac{h}{2}}\rho\left(\frac{\partial u_1}{\partial t}\,\delta\frac{\partial u_1}{\partial t} + \frac{\partial u_2}{\partial t}\,\delta\frac{\partial u_2}{\partial t}\right.$$
$$\left.+\frac{\partial u_3}{\partial t}\,\delta\frac{\partial u_3}{\partial t}\right)dzdA \quad (13)$$

By substituting the displacement field obtained in Eq. (1) into Eq. (13) then partial integration, the changes in kinetic energy obtained according to Eq. (14).

$$\delta T = \int_{A}\left(-I_0\frac{\partial^2 u_0}{\partial t^2}\delta u_0 + I_1\frac{\partial^3 u_0}{\partial x\partial t^2}\delta w_0\right.$$
$$-I_3\frac{\partial^2 u_0}{\partial t^2}\delta\phi_1 - I_1\frac{\partial^3 w_0}{\partial x\partial t^2}\delta u_0$$
$$+(I_2 + I_5)\frac{\partial^4 w_0}{\partial x^2\partial t^2}\delta w_0$$
$$-I_3\frac{\partial^2\phi_1}{\partial t^2}\delta u_0 + I_5\frac{\partial^3\phi_1}{\partial x\partial t^2}\delta w_0$$
$$-I_4\frac{\partial^2\phi_1}{\partial t^2}\delta\phi_1 - I_0\frac{\partial^2 v_0}{\partial t^2}\delta v_0$$
$$+\frac{I_1}{R}\frac{\partial^3 v_0}{\partial\theta\partial t^2}\delta w_0 + \frac{I_1}{R}\frac{\partial^2 v_0}{\partial t^2}\delta v_0$$
$$-I_3\frac{\partial^2 v_0}{\partial t^2}\delta\phi_2 - \frac{I_1}{R}\frac{\partial^3 w_0}{\partial\theta\partial t^2}\delta v_0$$
$$+\frac{I_2}{R^2}\frac{\partial^4 w_0}{\partial\theta^2\partial t^2}\delta w_0 \quad (14)$$
$$+\frac{I_2}{R^2}\frac{\partial^3 w_0}{\partial\theta\partial t^2}\delta v_0$$
$$-\frac{I_5}{R}\frac{\partial^3 w_0}{\partial\theta\partial t^2}\delta\phi_2 + \frac{I_1}{R}\frac{\partial^2 v_0}{\partial t^2}\delta v_0$$
$$-\frac{I_2}{R^2}\frac{\partial^3 v_0}{\partial\theta\partial t^2}\delta w_0$$
$$-\frac{I_2}{R^2}\frac{\partial^2 v_0}{\partial t^2}\delta v_0 + \frac{I_5}{R}\frac{\partial^2 v_0}{\partial t^2}\delta\phi_2$$
$$-I_3\frac{\partial^2\phi_2}{\partial t^2}\delta v_0 + \frac{I_5}{R}\frac{\partial^3\phi_2}{\partial\theta\partial t^2}\delta w_0$$
$$+\frac{I_5}{R}\frac{\partial^2\phi_2}{\partial t^2}\delta v_0 - I_4\frac{\partial^2\phi_2}{\partial t^2}\delta\phi_2$$
$$\left.-I_0\frac{\partial^2 w_0}{\partial t^2}\delta w_0\right)dA$$

Equation (14) expresses the mass moments as Eq. (15).

$$\{I_0, I_1, I_2, I_3, I_4, I_5\}$$
$$= \sum_{k=1}^{3} \int_{z_{k-1}}^{z_k} \rho^{(k)}\{1, f_1, f_1^2, f_2, f_2^2, f_1 f_2\}\, dz \qquad (15)$$

Equation (16) to Equation (20) express the governing equations in free vibration. They are obtained by substituting Eq. (10) and Eq. (14) into Eq. (7).

$$\delta u_0: \frac{\partial N_{xx}}{\partial x} + \frac{1}{R}\frac{\partial N_{x\theta}}{\partial \theta}$$
$$= I_0 \frac{\partial^2 u_0}{\partial t^2} + I_1 \frac{\partial^3 w_0}{\partial x \partial t^2} \qquad (16)$$
$$+ I_3 \frac{\partial^2 \phi_1}{\partial t^2}$$

$$\delta v_0: \frac{1}{R}\frac{\partial N_{\theta\theta}}{\partial \theta} - \frac{1}{R^2}\frac{\partial S_{\theta\theta}}{\partial \theta} + \frac{\partial N_{x\theta}}{\partial x} - \frac{1}{R}\frac{\partial S_{x\theta}}{\partial x}$$
$$+ \frac{T_{\theta z}}{R}$$
$$= \left(I_0 - \frac{2I_1}{R} + \frac{I_2}{R^2}\right)\frac{\partial^2 v_0}{\partial t^2} \qquad (17)$$
$$+ \left(\frac{I_1}{R} - \frac{I_2}{R^2}\right)\frac{\partial^3 w_0}{\partial \theta \partial t^2}$$
$$+ \left(I_3 - \frac{I_5}{R}\right)\frac{\partial^2 \phi_2}{\partial t^2}$$

$$\delta w_0: \frac{\partial T_{xz}}{\partial x} + \frac{1}{R}\frac{\partial T_{\theta z}}{\partial \theta} - \frac{\partial^2 S_{xx}}{\partial x^2} - \frac{1}{R^2}\frac{\partial^2 S_{\theta\theta}}{\partial \theta^2}$$
$$- \frac{N_{\theta\theta}}{R} - \frac{2}{R}\frac{\partial^2 S_{x\theta}}{\partial x \partial \theta}$$
$$= I_0 \frac{\partial^2 w_0}{\partial t^2} - I_1 \frac{\partial^3 u_0}{\partial x \partial t^2}$$
$$- (I_2 + I_5)\frac{\partial^4 w_0}{\partial x^2 \partial t^2} \qquad (18)$$
$$- I_5 \frac{\partial^3 \phi_1}{\partial x \partial t^2}$$
$$- \left(\frac{I_1}{R} - \frac{I_2}{R^2}\right)\frac{\partial^3 v_0}{\partial \theta \partial t^2}$$
$$- \frac{I_2}{R^2}\frac{\partial^4 w_0}{\partial \theta^2 \partial t^2} - \frac{I_5}{R}\frac{\partial^3 \phi_2}{\partial \theta \partial t^2}$$

$$\delta \phi_1: \frac{\partial P_{xx}}{\partial x} + \frac{1}{R}\frac{\partial P_{x\theta}}{\partial \theta} - Q_{xz}$$
$$= I_3 \frac{\partial^2 u_0}{\partial t^2} + I_4 \frac{\partial^2 \phi_1}{\partial t^2} \qquad (19)$$

$$\delta \phi_2: \frac{\partial P_{x\theta}}{\partial x} + \frac{1}{R}\frac{\partial P_{\theta\theta}}{\partial \theta} - Q_{\theta z}$$
$$= \left(I_3 - \frac{I_5}{R}\right)\frac{\partial^2 v_0}{\partial t^2} + \frac{I_5}{R}\frac{\partial^3 w_0}{\partial \theta \partial t^2} (20)$$
$$+ I_4 \frac{\partial^2 \phi_2}{\partial t^2}$$

Equation (16) to Equation (20) are in terms of the force components. The force and torque components from Eq. (11) should be reformulated in displacement terms to describe them accurately. Differentiated equations in terms of displacement are obtained in Appendix A.

3.4 Formulation of Liquid

This section describes how an incompressible, non-viscous liquid with a density of ρ_f behaves inside a cylindrical shell. Considering a non-rotating liquid, we establish the equations that describe its movement. In liquid-structure problems, waveforms are classified into two categories: bulging modes and sloshing modes. In bulging modes, the floor is assumed to be rigid, while the shell is assumed to be flexible. The vibration of the tank wall causes the natural frequency of bulging. Both the bottom and the shell are assumed to be rigid in sloshing modes, and the sloshing frequencies represent liquid fluctuations. The velocity potential of the liquid is denoted by $\overline{\emptyset}(x, \theta, r, t)$, and this velocity's potential must satisfy Laplace's Eq. (21) [21].

$$\frac{\partial^2 \overline{\emptyset}}{\partial r^2} + \frac{1}{r}\frac{\partial \overline{\emptyset}}{\partial r} + \frac{1}{r^2}\frac{\partial^2 \overline{\emptyset}}{\partial \theta^2} + \frac{\partial^2 \overline{\emptyset}}{\partial x^2} = 0 \qquad (21)$$

In this study, the potential of the liquid's velocity is considered harmonic and expressed by Eq. (22).

$$\overline{\emptyset}(x, \theta, r, t) = i\omega\, \emptyset(x, \theta, r)e^{i\omega t} \qquad (22)$$

Equation (22) defines $i^2 = -1$ and $\emptyset(x, \theta, r)$ as the potential of the liquid's displacement. By applying the superposition principle, the displacement's potential of the liquid can be expressed as the sum of the bulging-related displacement's potential and the sloshing-related displacement's potential, which is given by Eq. (23).

$$\emptyset = \emptyset^{(B)} + \emptyset^{(s)} \qquad (23)$$

In Eq. (23), $\emptyset^{(B)}$ and $\emptyset^{(s)}$ are bulging and sloshing displacement's potential, respectively. In this study, $\emptyset^{(B)}$ is the potential caused by the oscillation of a flexible cylindrical shell and rigid floor. At the same time, $\emptyset^{(s)}$ is generated by a rigid cylindrical shell and rigid floor. In order to obtain the liquid's potential, it is necessary to consider the boundary conditions.

$$at\ x = 0\quad \frac{\partial \emptyset^{(B)}}{\partial x} = 0 \qquad (24)\quad \frac{\partial \emptyset^{(s)}}{\partial x} = 0 \qquad (27)$$

$$at\ x = H\quad \emptyset^{(B)} = 0 \qquad (25)\quad \omega^2 \emptyset = g\frac{\partial \emptyset}{\partial x} \qquad (28)$$

$$at\ r = R\quad \frac{\partial \emptyset^{(B)}}{\partial r} = w(x, \theta, t) \ (26)\quad \frac{\partial \emptyset^{(s)}}{\partial r} = 0 \quad (29)$$

In Eq. (28), g represents the acceleration due to gravity on Earth. The boundary conditions are established based on the assumption that the vertical velocity is zero at the bottom of the tank for both bulging and sloshing potentials. For the bulging potential, the radial velocity of the liquid in the vicinity of the shell wall is equal to the shell velocity, and the dynamic pressure at the free surface of the fluid is zero. For the sloshing potential, the liquid velocity in the vicinity of the shell is assumed to be zero and at

the surface due to considering the shell as rigid. In the free surface, it is expressed as Eq. (28). By applying the principle of superposition, we can obtain Eq. (30) from the potentials in Eq. (28).

$$\omega^2 \emptyset^{(B)} = g \frac{\partial}{\partial x}(\emptyset^{(B)} + \emptyset^{(s)}) \quad at \quad (x = H) \quad (30)$$

To determine the liquid's potential response, we employed the method of separation of variables. Referring to Eq. (31), it can be expressed as follows:

$$\emptyset^{(B)} = R_1(r) \, \Theta(\theta) \, X(x) \tag{31}$$

By solving Eq. (31), the potential associated with bulging can be expressed as Eq.(32) [22, 23]

$$\emptyset^{(B)} = \sum_{m=1}^{M} \sum_{n=0}^{N} \left[\tilde{A}_{mn} \cos\left(\frac{(2m-1)\pi}{2H}x\right)\cos(n\theta) \right.$$
$$\left. I_n\left(\frac{(2m-1)\pi}{2H}r\right) \right] \tag{32}$$

In Eq. (32), the coefficients Amn represent unknown values. These coefficients are determined based on the remaining boundary condition associated with the flexible wall, given explicitly by Eq. (26).

According to the expansion of the Fourier series and Eq. (33), the coefficients $\tilde{A}_{mn}$ can be obtained in the form of Eq. (34) [23].

$$\sum_{m=1}^{M} \sum_{n=0}^{N} \left[\tilde{A}_{mn} \frac{(2m-1)\pi}{2H} \cos\left(\frac{(2m-1)\pi}{2H}x\right) \right.$$
$$\left. \cos(n\theta) \, I'_n\left(\frac{(2m-1)\pi}{2H}R\right) \right] = w(x,\theta) \tag{33}$$

$$\tilde{A}_{mn} = \frac{\frac{coff}{2\pi R H}}{\frac{(2m-1)\pi}{2H} \, I'_n\left(\frac{(2m-1)\pi}{2H}R\right)} \tag{34}$$
$$\int_0^H \int_0^{2\pi} \cos\left(\frac{(2m-1)\pi}{2H}x\right)\cos(n\theta)\,Rd\theta dx,$$

where:

$$coff = \begin{cases} 1 & if \ m = n = 0 \\ 2 & if \ m \ or \ n = 0 \\ 4 & if \ m \ and \ n \neq 0 \end{cases}$$

Using a similar method and considering the boundary conditions related to liquid sloshing, the potential function of liquid sloshing can be expressed as Eq. (35).

$$\emptyset^{(s)} = \sum_{k=1}^{K} \sum_{n=0}^{N} \tilde{B}_{nk} \cosh\left(\frac{\varepsilon_{nk}}{R}x\right)\cos(n\theta) J_n\left(\frac{\varepsilon_{nk}}{R}r\right) \tag{35}$$

In Eq. (35), according to the liquid sloshing boundary conditions, Eq. (36) can obtain.

$$\frac{d J_n\left(\frac{\varepsilon_{nk}}{R}r\right)}{dr} = 0 \quad at \quad (r = R) \tag{36}$$

The fluid's kinetic energy can be expressed as Eq. (37), considering that the liquid in question is an incompressible liquid [22].

$$T_f = \frac{1}{2} \, \rho_f \omega^2 \iint_S \emptyset \, \frac{\partial \emptyset}{\partial n} \, dS \tag{37}$$

Equation (38) expresses the changes in the kinetic energy of the liquid. Let ρ_f be the density of the liquid, n is the normal of the associated surface, and S is the surface associated with the integration.

$$\delta T_f = \frac{1}{2} \, \rho_f \omega^2 \int_0^H \int_0^{2\pi} (\emptyset^{(B)}|_{r=R} + \emptyset^{(s)}|_{r=R})\delta w \, Rd\theta dx \tag{38}$$

3.5 Investigating the Impact of Liquid on Structure Vibration

If we consider a cylindrical shell containing liquid, Hamilton's principle can be rewritten as Eq. (39)[24].

$$\int_0^t (\delta T_{shell} + \delta T_{fluid} - \delta U_{shell})dt = 0 \tag{39}$$

Given that the changes in the kinetic energy of the liquid are proportional to δw, the fluid in the cylindrical shell affects the δw equation while leaving the other obtained equations unchanged. Eq. (18) modified to Eq. (40).

The presentation of relations 16, 17, 19, 20, and 40 for sandwich cylindrical shells with an auxetic core, along with the consideration of fluid presence, can serve as a valuable resource for future studies related to this topic.

$$\delta w_0 : (E_3 + E_4)\frac{\partial \phi_1}{\partial x} + (E_1 + 2E_2 + E_5)\frac{\partial^2 w_0}{\partial x^2} + \frac{1}{R}\left((D_3 + D_4)\frac{\partial \phi_2}{\partial \theta} + \frac{(D_1 + 2D_2 + D_5)}{R}\left(\frac{\partial^2 w_0}{\partial \theta^2} - \frac{\partial v_0}{\partial \theta}\right)\right)$$

$$- \frac{A_3}{R}\left(\frac{\partial^3 v_0}{\partial x^2 \partial \theta} + \frac{\partial^2 w_0}{\partial x^2}\right) - \frac{A_4}{R}\frac{\partial^3 \phi_2}{\partial x^2 \partial \theta} - \frac{A_5}{R^2}\left(\frac{\partial^4 w_0}{\partial x^2 \partial \theta^2} - \frac{\partial^3 v_0}{\partial x^2 \partial \theta}\right) - B_3\frac{\partial^3 u_0}{\partial x^3} - B_4\frac{\partial^3 \phi_1}{\partial x^3} - B_5\frac{\partial^4 w_0}{\partial x^4}$$

$$- \frac{1}{R^2}\left(\frac{F_3}{R}\left(\frac{\partial^3 v_0}{\partial \theta^3} + \frac{\partial^2 w_0}{\partial \theta^2}\right) + \frac{F_4}{R}\frac{\partial^3 \phi_2}{\partial \theta^3} + \frac{F_5}{R^2}\left(\frac{\partial^4 w_0}{\partial \theta^4} - \frac{\partial^3 v_0}{\partial \theta^3}\right) + A_3\frac{\partial u_0}{\partial x} + A_4\frac{\partial^3 \phi_1}{\partial x \partial \theta^2} + A_5\frac{\partial^4 w_0}{\partial x^2 \partial \theta^2}\right)$$

$$- \frac{1}{R}\left(\frac{F_1}{R}\left(\frac{\partial v_0}{\partial \theta} + w_0\right) + \frac{F_2}{R}\frac{\partial \phi_2}{\partial \theta} + \frac{F_3}{R^2}\left(\frac{\partial^2 w_0}{\partial \theta^2} - \frac{\partial v_0}{\partial \theta}\right) + A_1\frac{\partial u_0}{\partial x} + A_2\frac{\partial \phi_1}{\partial x} + A_3\frac{\partial^2 w_0}{\partial x^2}\right) \qquad (40)$$

$$- \frac{2}{R}\left(C_3\frac{\partial^3 v_0}{\partial x^2 \partial \theta} + C_4\frac{\partial^3 \phi_2}{\partial x^2 \partial \theta} + \frac{C_5}{R}\left(2\frac{\partial^4 w_0}{\partial x^2 \partial \theta^2} - \frac{\partial^3 v_0}{\partial x^2 \partial \theta}\right) + \frac{C_3}{R}\frac{\partial^3 u_0}{\partial x \partial \theta^2} + \frac{C_4}{R}\frac{\partial^3 \phi_1}{\partial x \partial \theta^2}\right)$$

$$= I_0\frac{\partial^2 w_0}{\partial t^2} - I_1\frac{\partial^3 u_0}{\partial x \partial t^2} - (I_2 + I_5)\frac{\partial^4 w_0}{\partial x^2 \partial t^2} - I_5\frac{\partial^3 \phi_1}{\partial x \partial t^2} - \left(\frac{I_1}{R} - \frac{I_2}{R^2}\right)\frac{\partial^3 v_0}{\partial \theta \partial t^2} - \frac{I_2}{R^2}\frac{\partial^4 w_0}{\partial \theta^2 \partial t^2} - \frac{I_5}{R}\frac{\partial^3 \phi_2}{\partial \theta \partial t^2}$$

$$- \frac{1}{2}\rho_f \omega^2(\emptyset^{(B)}|_{r=R} + \emptyset^{(s)}|_{r=R})$$

4. Solution Procedure Using the Galerkin Approach

This study used the Galerkin numerical solution method to solve the assumed system based on the boundary conditions used for the problem. Eq. (41) represents the proposal functions used to solve the equations of motion and obtain u, v, w, ϕ_1, and ϕ_2.

$$u_0(x, \theta) = \sum_{\widetilde{m}=1}^{\bar{M}} \sum_{\widetilde{n}=1}^{\bar{N}} u_{\widetilde{m}\widetilde{n}}\bar{\bar{u}}_0(x, \theta)$$

$$v_0(x, \theta) = \sum_{\widetilde{m}=1}^{\bar{M}} \sum_{\widetilde{n}=1}^{\bar{N}} v_{\widetilde{m}\widetilde{n}}\bar{\bar{v}}_0(x, \theta)$$

$$w_0(x, \theta) = \sum_{\widetilde{m}=1}^{\bar{M}} \sum_{\widetilde{n}=1}^{\bar{N}} w_{\widetilde{m}\widetilde{n}}\bar{\bar{w}}_0(x, \theta) \qquad (41)$$

$$\phi_1(x, \theta) = \sum_{\widetilde{m}=1}^{\bar{M}} \sum_{\widetilde{n}=1}^{\bar{N}} \phi_{1_{\widetilde{m}\widetilde{n}}}\bar{\bar{\phi}}_1(x, \theta)$$

$$\phi_2(x, \theta) = \sum_{\widetilde{m}=1}^{\bar{M}} \sum_{\widetilde{n}=1}^{\bar{N}} \phi_{2_{\widetilde{m}\widetilde{n}}}\bar{\bar{\phi}}_2(x, \theta)$$

where $u_{\widetilde{m}\widetilde{n}}$, $v_{\widetilde{m}\widetilde{n}}$, $w_{\widetilde{m}\widetilde{n}}$, $\phi_{1_{\widetilde{m}\widetilde{n}}}$, and $\phi_{2_{\widetilde{m}\widetilde{n}}}$ are unknown coefficients obtained by minimizing the errors.

$\bar{\bar{u}}_0(x, \theta), \bar{\bar{v}}_0(x, \theta), \bar{\bar{w}}_0(x, \theta), \bar{\bar{\phi}}_1(x, \theta)$, and $\bar{\bar{\phi}}_2(x, \theta)$ are functions that must satisfy the necessary boundary conditions and are considered as the weight functions in the Galerkin method. The cylindrical shell is investigated in two boundary conditions: both ends with simple support and clamped support. So, the trial functions will be Eq. (42) and Eq. (43).

$$\begin{cases} \bar{\bar{u}}_0(x, \theta) = \cos(\alpha_{\widetilde{m}}x)\cos(\widetilde{n}\theta) \\ \bar{\bar{v}}_0(x, \theta) = \sin(\alpha_{\widetilde{m}}x)\sin(\widetilde{n}\theta) \\ \bar{\bar{w}}_0(x, \theta) = \sin(\alpha_{\widetilde{m}}x)\cos(\widetilde{n}\theta) \\ \bar{\bar{\phi}}_1(x, \theta) = \cos(\alpha_{\widetilde{m}}x)\cos(\widetilde{n}\theta) \\ \bar{\bar{\phi}}_2(x, \theta) = \sin(\alpha_{\widetilde{m}}x)\sin(\widetilde{n}\theta) \end{cases} \text{for } S-S \quad (42)$$

$$\begin{cases} \bar{\bar{u}}_0(x, \theta) = \sin(2\alpha_{\widetilde{m}}x)\cos(\widetilde{n}\theta) \\ \bar{\bar{v}}_0(x, \theta) = \sin^2(\alpha_{\widetilde{m}}x)\sin(\widetilde{n}\theta) \\ \bar{\bar{w}}_0(x, \theta) = \sin^2(\alpha_{\widetilde{m}}x)\cos(\widetilde{n}\theta) \\ \bar{\bar{\phi}}_1(x, \theta) = \sin(2\alpha_{\widetilde{m}}x)\cos(\widetilde{n}\theta) \\ \bar{\bar{\phi}}_2(x, \theta) = \sin^2(\alpha_{\widetilde{m}}x)\sin(\widetilde{n}\theta) \end{cases} \text{for } C-C \quad (43)$$

Let $\widetilde{n}$ and $\widetilde{m}$ denote the longitudinal and circumferential half-wave numbers, respectively. Additionally, we assumed $\alpha_{\widetilde{m}} = \frac{\widetilde{m}\pi}{L}$, where L represents the characteristic length. Furthermore, ω signifies the natural frequency of the system. By applying the Galerkin weighted residual method to the equations of motion and minimizing the error, we obtained the eigenvalue problem in Eq. (44).

$$([\boldsymbol{K}] - \omega^2[\boldsymbol{M}])\{\boldsymbol{\Lambda}\} = \{0\} \qquad (44)$$

In this context, $\{\boldsymbol{\Lambda}\}$, $[\boldsymbol{K}]$, and $[\boldsymbol{M}]$ represent the vector of constants, the stiffness and mass matrices, respectively. The natural frequencies of the system can be obtained by solving the Eq. (44).

5. Validation Studies

The numerical results of analyzing the three-layer cylindrical body filled with liquid and an auxetic core are presented in this section. We used the Galerkin weighted residual solution method and solved equations. The cylindrical shell is considered under two boundary conditions: both ends simple support and clamped support. We used the modified high-order shear deformation theory to model the system's mechanical behavior. All numerical results presented in this article were obtained by using MATLAB. We compared the theoretical solution of the problem with the results presented in authoritative references (which will be stated below) and the finite element analysis in ABAQUS. We investigated the influence of different geometrical parameters of the body,

liquid interaction, and the effective parameters of the auxetic core on the system's responses. The three-layered cylindrical shell comprises isotropic inner and outer surfaces made of aluminum, with a honeycomb auxetic structure serving as the core within the same aluminum material. Poisson's ratio and Young's modulus for aluminum are 0.3 and 70 × 10^9 (Pa), respectively. Table 2 presents the material and geometric properties considered for an auxetic cell.

To verify the accuracy of the theoretical results, we analyzed the cylindrical shell in ABAQUS. Table 3 presents the natural frequency values obtained for the system according to the size and type of mesh. The results demonstrate

convergence. Based on the recorded values, quadratic elements with a size of 0.03 are chosen as the most suitable type and size of the mesh to record the results.

This study indicates the convergence in natural frequencies of cylindrical shells, and harmonic responses were considered. Table 4 and Figure 3 demonstrate this convergence. Based on these data, the m and n values that cause the convergence of the first to sixth modes can be identified. By choosing m and n equal to 6, the first to sixth natural frequencies converge with the acceptable error percentage.

Table 2: Properties of Auxetic Core Unit Cell for ABAQUS Analysis

$E_1^{(2)}$(Pa)	$E_2^{(2)}$(Pa)	$G_{12}^{(2)}$(Pa)	$G_{13}^{(2)}$(Pa)	$G_{23}^{(2)}$(Pa)	$v_{12}^{(2)}$
680465	203697	8.86784×10^7	5.10105×10^7	2.04042×10^8	-1.82632
$v_{21}^{(2)}$	$\rho^{(2)}(\frac{Kg}{m^3})$	η_1	η_2	η_3	$\frac{h_c}{h}$
-0.546708	81.85	2	1	0.0138571	0.33333

Table 3: Convergence of Natural Frequencies for the First Mode Shape Based on Mesh Size and Type in ABAQUS

Geometric Order	Approximate Global Size					
	0.5	0.3	0.2	0.1	0.05	0.03
Linear	37.37	33.82	32.69	32.13	32.03	32.00
Quadratic	32.41	32.14	32.07	32.04	32.026	32.01

Table 4: Convergence of the Galerkin Method Assessment

| Frequency number	$m = n = 1$	$m = n = 2$	$m = n = 3$	$m = n = 4$	$m = n = 5$	$m = n = 6$	$m = n = 7$
1	118.7578	46.6411	32.13126	32.13126	32.13126	32.13126	32.13126
2	636.1324	118.7578	46.6411	45.23311	46.6411	46.6411	46.6411
3	1231.754	153.6774	86.28209	67.62597	67.62597	67.62597	67.62597
4	105325.8	314.5121	118.7578	67.62597	67.62597	67.62597	67.62597
5	105740.6	636.1324	153.6774	86.28209	70.05918	70.05918	70.05918
6		861.8646	116.0653	115.1534	79.10043	79.10043	79.10043
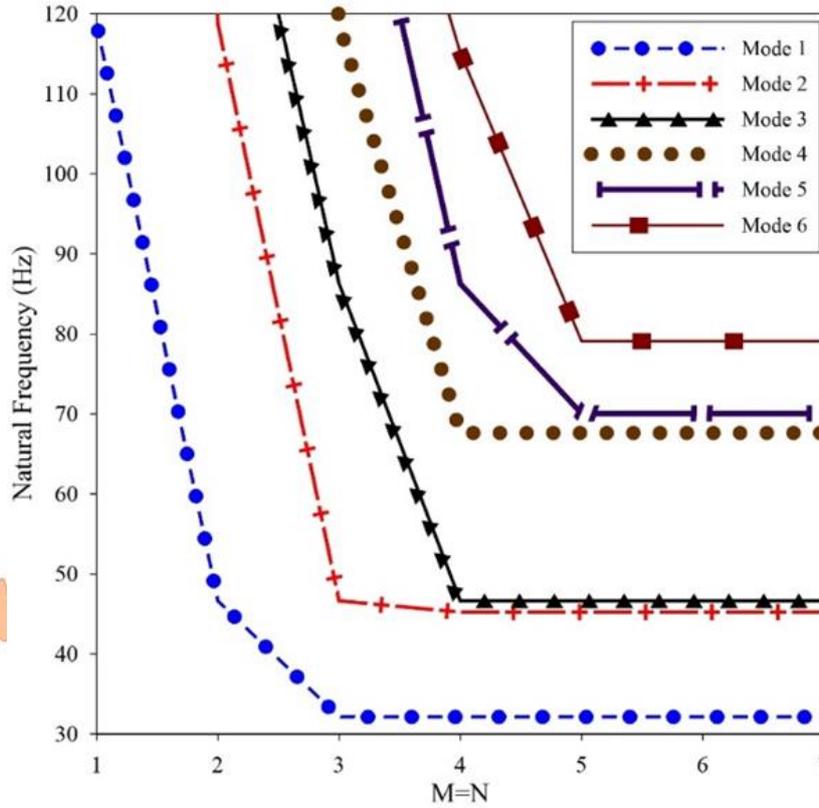
Fig. 3: Convergence of the Galerkin Method for a Three-Layer Cylindrical Shell with an Auxetic Core

Table 5 presents the dimensionless natural frequency values for ten primary mode shapes and considers the simple support's boundary conditions. This table compares the results of this study with reference articles. Table 6 provides data similar to that in Table 5 for a cylindrical shell with clamped support (CC). Tables 7 and 8 provide dimensionless natural frequency values for a relatively thick cylindrical structure. Table 7 corresponds to the case of simple support, whereas Table 8 pertains to the condition of clamped support.

Table 5: Dimensionless Natural Frequencies for Homogeneous Cylindrical Shell (Simple Supported at Both Ends) ($\tilde{\omega} = \omega R \sqrt{\frac{(1-\upsilon^2)\rho}{E}}$)

	$(m = 1, \frac{L}{R} = 20, \frac{h}{R} = 0.01, \nu = 0.3)$									
Methods	n									
	1	2	3	4	5	6	7	8	9	10
Reference [25]	0.016101	0.009382	0.022105	0.042095	0.068008	0.09973	0.137239	0.180527	0.229594	0.284433
Reference [26]	0.016103	0.009388	0.022108	0.042097	0.06008	0.09973	0.137239	0.180528	0.229594	0.284436
ESDPT (Present work)	0.0161023	0.00938704	0.0221048	0.0420848	0.0679784	0.099656	0.137117	0.180318	0.229256	0.283918
TSDPT (Present work)	0.0161023	0.00938703	0.0221048	0.0420848	0.0679783	0.0996653	0.137117	0.180317	0.229254	0.283916
HSDPT (Present work)	0.0161023	0.00938703	0.0221048	0.0420848	0.0679782	0.0996653	0.137117	0.180317	0.229254	0.283915
PSDPT (Present work)	0.0161023	0.00938703	0.0221048	0.0420848	0.0679782	0.0996653	0.137117	0.180317	0.229254	0.283915

Table 6 : Dimensionless Natural Frequencies ($\tilde{\omega}$) for Homogeneous Cylindrical Shell with Clamped Supports (CC)

	$(m = 1, \frac{L}{R} = 20, \frac{h}{R} = 0.01, \nu = 0.3)$									
Methods	n									
	1	2	3	4	5	6	7	8	9	10
Reference [25]	0.032885	0.013932	0.022672	0.042208	0.068046	0.099748	0.137249	0.180535	0.229599	0.284439
Reference [26]	0.033176	0.01397	0.022677	0.04221	0.068048	0.099749	0.13725	0.180535	0.2296	0.284441
ESDPT (Present work)	0.0351121	0.0144509	0.0227473	0.0422178	0.0680299	0.0996981	0.137144	0.180343	0.22928	0.283941

TSDPT (Present work)	0.0351121	0.0144509	0.0227473	0.0422178	0.0680298	0.0996979	0.137144	0.180342	0.229279	0.28394
HSDPT (Present work)	0.0351121	0.0144509	0.0227473	0.0422178	0.0680297	0.0996978	0.137144	0.180342	0.229278	0.283939
PSDPT (Present work)	0.0351121	0.0144509	0.0227473	0.0422178	0.0680297	0.0996978	0.137144	0.180342	0.229278	0.283939

Table 7: Dimensionless Natural Frequencies of a Relatively Thick Cylindrical Shell with Simply Support (SS)

$\dfrac{L}{R}$	$m = 1 , \dfrac{h}{R} = 0.1 , v = 0.3$			
		$n = 1$	$n = 2$	$n = 3$	$n = 4$
2	Present work	0.03099	0.01914	0.01824	0.02617
	Reference [27]	0.03099	0.01911	0.01820	0.02617
1	Present work	0.04791	0.03985	0.03659	0.04054
	Reference [27]	0.04790	0.03982	0.03655	0.04055
0.5	Present work	0.07622	0.07682	0.07921	0.08441
	Reference [27]	0.07648	0.07713	0.07959	0.08494

Table 8: Dimensionless Natural Frequencies of a Relatively Thick Cylindrical Shell with Clamped Ends (CC)

$\dfrac{h}{L}$	$m = 1 , h/R = 0.2 , v = 0.3$			
		$n = 0$	$n = 1$	$n = 2$
0.1	Reference [27]	1.03567	0.70965	0.58328
	Reference [28]	1.03567	0.69319	0.56971
	ESDPT	1.02958	0.685409	0.559965
	TSDPT	1.0297	0.0685449	0.0559955
	HSDPT	1.02516	0.683292	0.557878
	PSDPT	1.03088	0.685996	0.560461
0.2	Reference [27]	1.49180	1.41950	1.36752
	Reference [28]	1.47766	1.39567	1.33769
	ESDPT	1.44844	1.36595	1.30682
	TSDPT	1.44853	1.36591	1.30661
	HSDPT	1.42306	1.34369	1.2857
	PSDPT	1.45491	1.3714	1.30661

The purpose of the previously presented tables is to validate the derived equations of motion within the study report. To compute the natural frequencies for a three-layered cylindrical cover with an auxetic core, we define its specifications as outlined in Table 9.

Tables 10 and 11 present dimensionless natural frequency values for the system. Table 10 is for the condition of simple support, while Table 11 is for the condition of clamped support. A finite element analysis has been conducted to verify the accuracy of these natural frequency values.

Table 12 and Table 13 present the natural frequency values of the system with liquid. Table 12 corresponds to the bulging mode condition. The cylinder, liquid, and support have these characteristics: radius = 0.9 (m), radius to thickness ratio = 60, length to radius ratio = 98.24, density = 7812 (kg/m^3), Poisson's ratio = 0.3, Young's modulus = 203.4×10^9 (Pa). The liquid is water (Non-viscous and incompressible) with a density of 1000 (kg/m^3). The support condition is simple support [29].

In the next step, we assume that the fluid is water and the support condition is simply support. The geometric characteristics of the cylinder are as follows: radius = 25 (m), length = 30 (m), thickness = 0.03 (m), density = 7850 (kg/m^3), Poisson's ratio = 0.3, and Young's modulus = 206×10^9 (Pa). The height of water in the tank is 21.6 (m). The natural frequency values for both bulging and sloshing modes are calculated and presented in Table 13 [30].

Table 9: Properties of Three-Layer Shells with Auxetic Cores for ABAQUS Modeling

$E_1^{(2)}(Pa)$	$E_2^{(2)}(Pa)$	$G_{12}^{(2)}(Pa)$	$G_{13}^{(2)}(Pa)$	$G_{23}^{(2)}(Pa)$	$v_{12}^{(2)}$	$v_{21}^{(2)}$	$\rho^{(2)}(Kg/m^3)$
680465	203697	8.86784×10^7	5.10105×10^7	2.04045×10^8	-1.82632	-0.546708	81.85
η_2	η_2	η_3	h_c/h	h/R	L/R	v	E

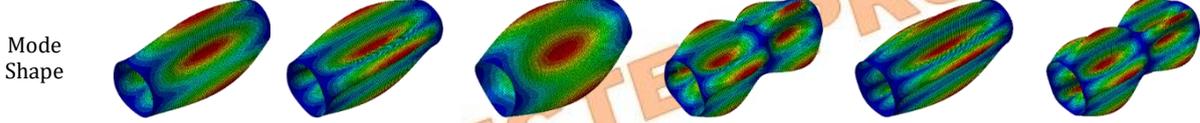| 2 | 1 | 0.0138571 | 0.0033333 | 0.01 | 6 | 0.3 | 70×10^9 |

Table 10: Dimensionless Natural Frequency Comparison: Mathematical Equations vs. ABAQUS Output (SS Condition)

	First mode (1,3)	Second mode (1,4)	Third mode (1,2)	Fourth mode (2,4)	Fifth mode (1,5)	Sixth mode (2,5)
			Number of modes (m,n)			
FEM	0.0608	0.0847	0.0886	0.1275	0.1300	0.1471
ESDPT	0.06105	0.0859	0.0886	0.1285	0.1331	0.1503
TSDPT	0.06105	0.0859	0.0886	0.1285	0.1331	0.1503
HSDPT	0.06105	0.0859	0.0886	0.1285	0.1331	0.1503
PSDPT	0.06105	0.0859	0.0886	0.1285	0.1331	0.1503
Mode Shape						

Table 11: Dimensionless Natural Frequency Comparison: Mathematical Equations vs. ABAQUS Output (CC Condition)

	First Mode (1,3)	Second Mode (1,4)	Third Mode (1,5)	Fourth Mode (1,2)	Fifth Mode (2,4)
			Number of modes(m,n)		
FEM	0.003187	0.003219	0.004463	0.005191	0.005226
PSDPT	0.00327364	0.003282825	0.004575305	0.0053867	0.005675905
Mode Shape					
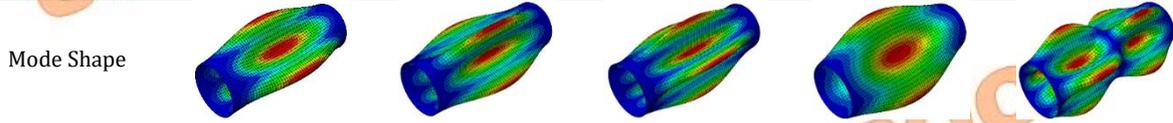
Table 12: Natural Frequencies (Hz) of an Isotropic Cylindrical Shell Immersed in Incompressible Liquid

	1	2	3	4
		m		
Reference [29]	4.549	17.46	37.137	62.115
Reference [31]	4.5504	17.257	36.361	59.594
ESDPT (Present Work)	4.519	17.308	36.491	59.964
THDPT (Present Work)	4.519	17.308	36.491	59.964
HSDPT (Present Work)	4.519	17.308	36.491	59.964
PSDPT (Present Work)	4.519	17.308	36.491	59.964

Table 13: Natural Frequency Values (rad/s) for Sloshing and Bulging in a Cylindrical Shell Containing Liquid (n=4)

	Sloshing					Bulging				
	$m=1$	$m=2$	$m=3$	$m=4$	$m=5$	$m=1$	$m=2$	$m=3$	$m=4$	$m=5$
Reference[21]	1.4426	1.9081	2.2305	2.5027	2.7444	14.054	34.672	49.629	61.556	71.476
Reference[30]	1.4425	1.9081	2.2305	2.5027	2.7444	13.658	34.441	49.692	61.877	71.804
PSDPT (Present Work)	1.44363	1.90754	2.22964	2.50159	2.74314	14.3794	36.7664	48.9498	59.2963	70.5365

6. Discussion

6.1. Impact of Shell Geometric Parameters on Natural Frequency

The L/R ratio's influence on the natural frequencies of a three-layer cylindrical shell with an auxetic core is examined in Figure 4. The study considers two boundary conditions: simply support at both ends and clamped support at both ends. Material and geometric properties align with Table 2, revealing the following trends:

1. Clamped Support vs. Simply Support:
The shell with both-ends clamped support exhibits a higher natural frequency than the shell with simply support. This difference arises due to the additional constraints in the clamped support configuration.

2. Effect of Shell Length:
- In both boundary conditions, natural frequencies decrease as the shell length increases. This decrease is attributed to an increase in the system's mass and a reduction in the stiffness-to-mass ratio.
- Interestingly, boundary conditions have fewer impact frequencies in longer shells. However, in shorter shells, boundary conditions significantly affect natural frequencies.

12

- The slope of the natural frequency graph is much steeper in shorter shells than in longer ones.

3. Critical Length-to-Radius Ratio:

Beyond a particular value of the length-to-radius ratio, changes in this ratio have minimal impact on natural frequencies, resulting in a horizontal trend in the graph.
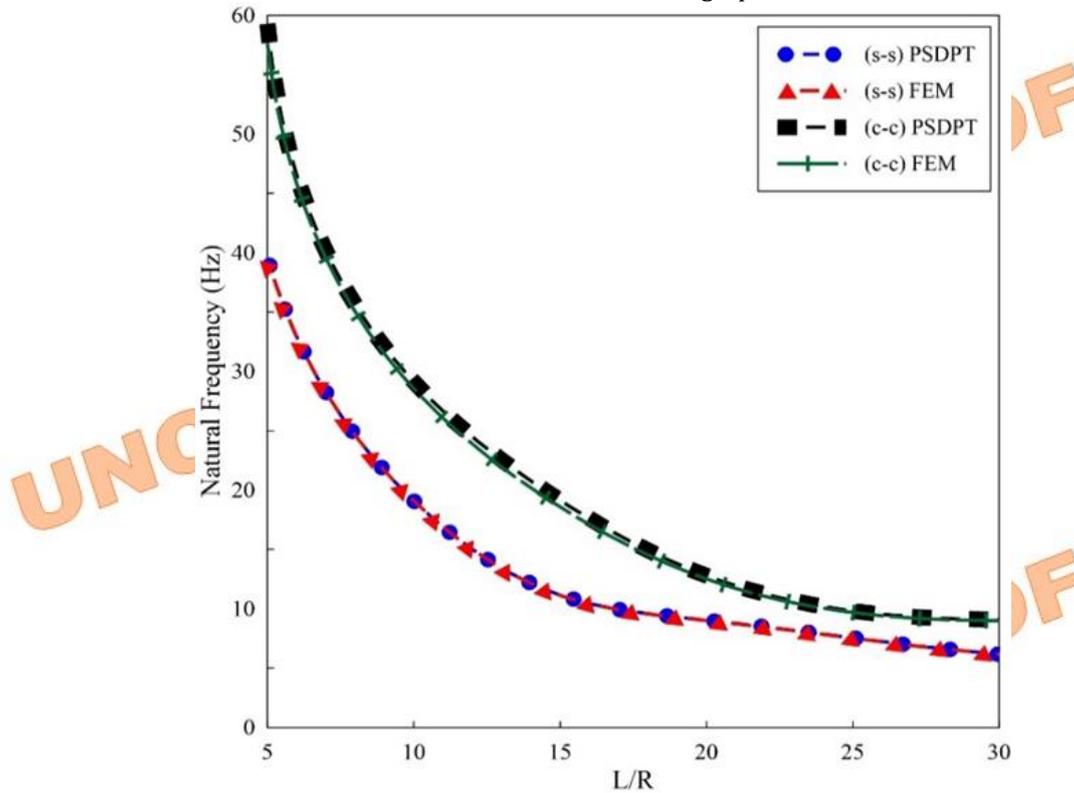

Fig. 4: Impact of Shell Length-to-Radius Ratio on Fundamental Natural Frequency in a Three-Layer Shell with Auxetic Core

Figure 5 investigates the impact of the overall thickness of the shell on natural frequencies under two boundary conditions: simply support and clamped support. The material and geometric properties of the shell align with Table 2. The key findings are as follows:

1. Clamped Support vs. Simply Support:
Shells with both ends clamped support exhibit more significant natural frequencies than those with simple support. The additional constraints in the clamped support configuration contribute to this difference.

2. Effect of Shell Thickness:
- In both boundary conditions, natural frequencies increase as the shell thickness grows. This increase is attributed to the system's stiffness enhancement.
- As shell thickness increases, the influence of boundary conditions becomes more pronounced. Conversely, thinner shells are less affected by these conditions.

3. Slope of the System:
With increasing shell thickness, the slope of the natural frequency graph decreases until further thickness variations have minimal impact. At this stage, the graph tends to become horizontal.

6.2. The Influence of Geometrical Parameters of the Core on Natural Frequencies

Figure 6 examines how the core thickness affects the natural frequencies of three-layer shells with auxetic cores. These shells have different thickness ratios (h/R) and are simply supported at both ends. Here are the key findings:
1. **Thicker Shells**: Thicker shells exhibit more pronounced natural frequencies when the core thickness increases. This is because the stiffness-to-mass ratio of thicker shells is higher, leading to enhanced natural frequencies

2. **Thin Shells (h/R = 0.01 and 0.05)**: In thin shells, the natural frequency increases with a gentler slope than in thick shells. However, the natural frequency decreases when the core

13

thickness reaches 80% of the total thickness.

3. **Thin Cylindrical Shells (h/R = 0.01)**: Increasing the core thickness has minimal impact on the natural frequency. Only when the core thickness reaches 80% of the total thickness does it exhibit a maximum and downward trend."
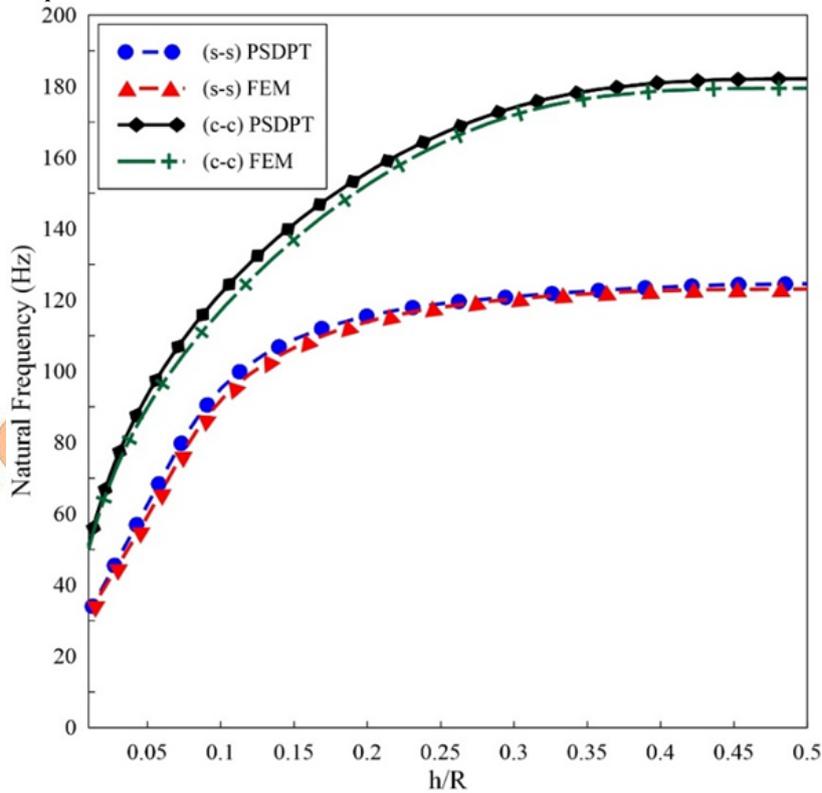

Fig. 5: Impact of Overall Shell Thickness on Fundamental Natural Frequency in a Three-Layer Shell with Auxetic Core
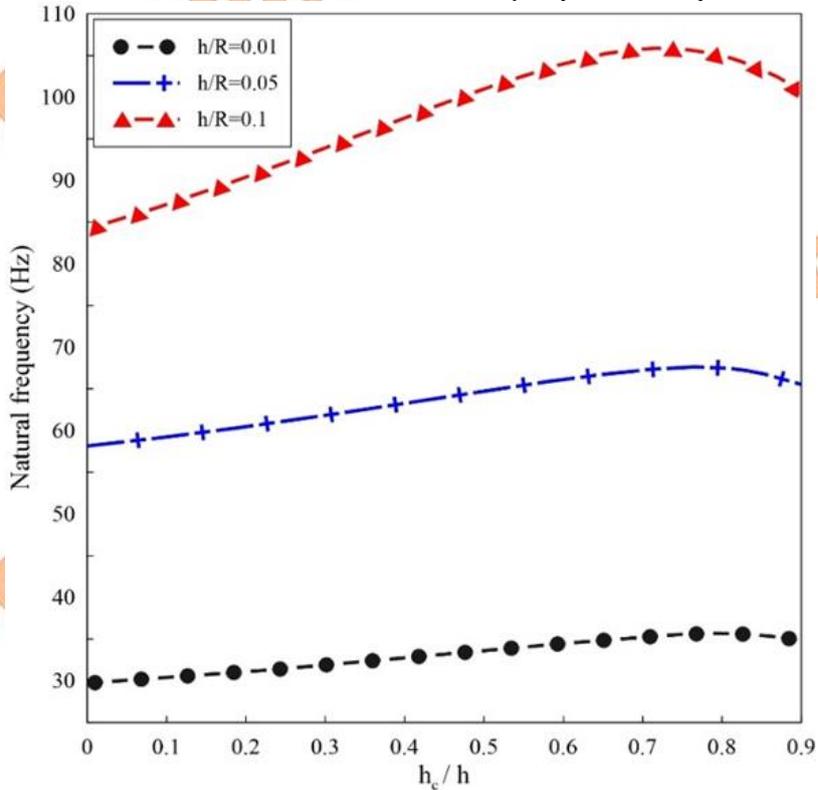

Fig. 6: Core Thickness Ratio and Natural Frequencies in Thin and Relatively Thick Shells

Figure 7 investigates the impact of a core thickness (h_c) in a thick cylindrical shell with simply support boundary conditions and varying L/R ratios (assuming that h is constant). Here are the key findings:

1. Natural Frequency Increase: As the shell length decreases, the natural frequencies increase due to reduced mass and a higher stiffness-to-mass ratio.
2. Maximum Natural Frequency: Similar to Figure 6, the maximum natural frequency occurs when the core thickness is 70% of the total thickness. Beyond this point, the natural frequencies decrease.
3. L/R Ratio Independence: The rate of rise and fall of the natural frequency graphs does not depend on the value of L/R. Length ratios of 15 and more have minimal effect on natural frequency.

Figure 8 illustrates the impact of changing θ on the behavior of a thin and isotropic single-layer shell made of base metal in terms of natural frequencies. Here are the key findings:

1. Lowest Natural Frequency: The thin single-layer shell exhibits the lowest natural frequency.

2. Impact of Auxetic Layer Thickness (h_c):
- As the auxetic layer thickens, the system's natural frequency increases when the angle θ falls between -70 and -40.
- However, when the ratio h_c/h reaches the optimal value of 75%, the natural frequency decreases.
3. Stable Trend for Negative Angles:
- The natural frequency increases steadily for negative angles with values less than 40.
- Interestingly, changes in the cell angle of the auxetic structure have minimal effect on the natural frequency when h_c/h is smaller than 0.3

Similar to Figure 8, Figure 9 illustrates the impact of changing the angle in cells of the auxetic layer but in a thick shell. The natural frequency continues to increase with the thickness of the auxetic layer up to the optimal value of 65% to 75%. Beyond this range, the natural frequency decreases as the ratio of h_c/h increases. the natural frequency starts to decrease. This trend holds for all θ angles.
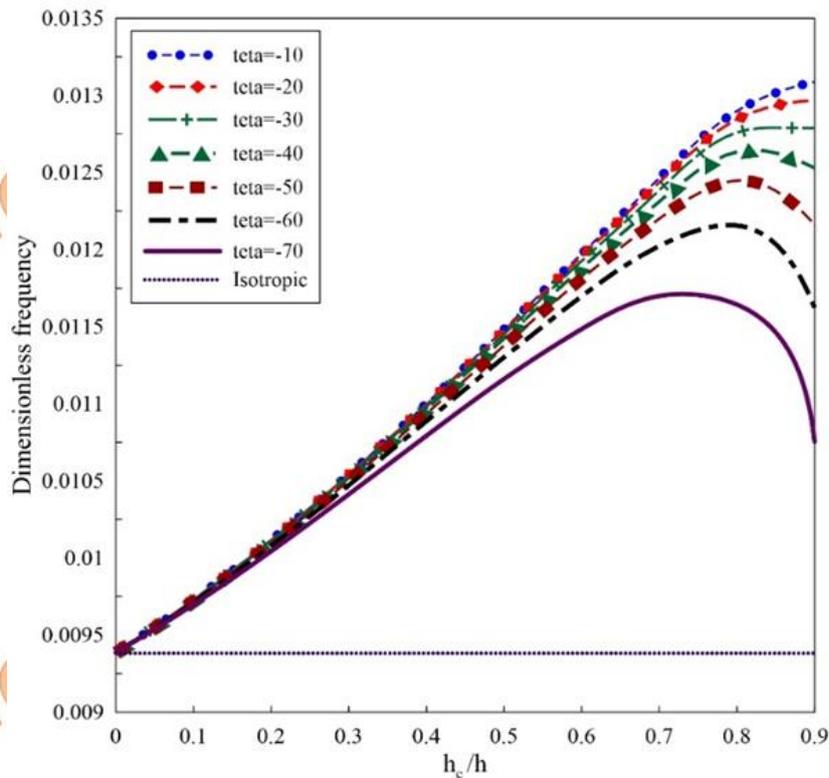

Fig. 8: Effect of Thin Shell Core Thickness and Auxetic Unit Cell Angle on Natural Frequencies
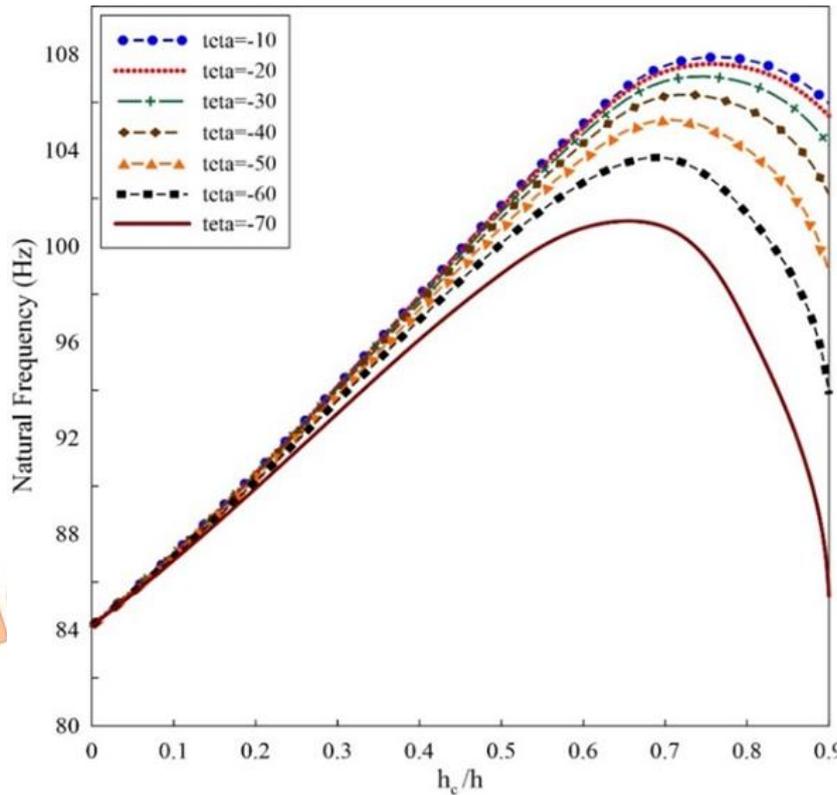
Fig. 9: Influence of Core Thickness and Auxetic Unit Cell Angle on Natural Frequencies in Relatively Thick Shell Structures

6.3. Liquid Structures Interaction:

Figure 10 illustrates the impact of liquid height within a cylindrical shell composed of three vertical layers with both ends simple support; considering various mode shapes as the tank is gradually filled with the assumed fluid, the system's mass increases. Consequently, this increase in mass leads to a reduction in the natural frequencies across different modes.

Figure 11 illustrates the influence of liquid density within a three-layer cylindrical shell with an auxetic core on the system's natural frequencies. Due to increased liquid density, the system's mass gradually rises while the system's stiffness remains constant. Consequently, this increase in mass leads to a reduction in the natural frequencies. Notably, as the density of the liquid inside the cylindrical shell further increases, the natural frequencies exhibit a diminishing trend with a gentler slope. Remarkably, the natural frequency remains consistently stable for liquids with high density.
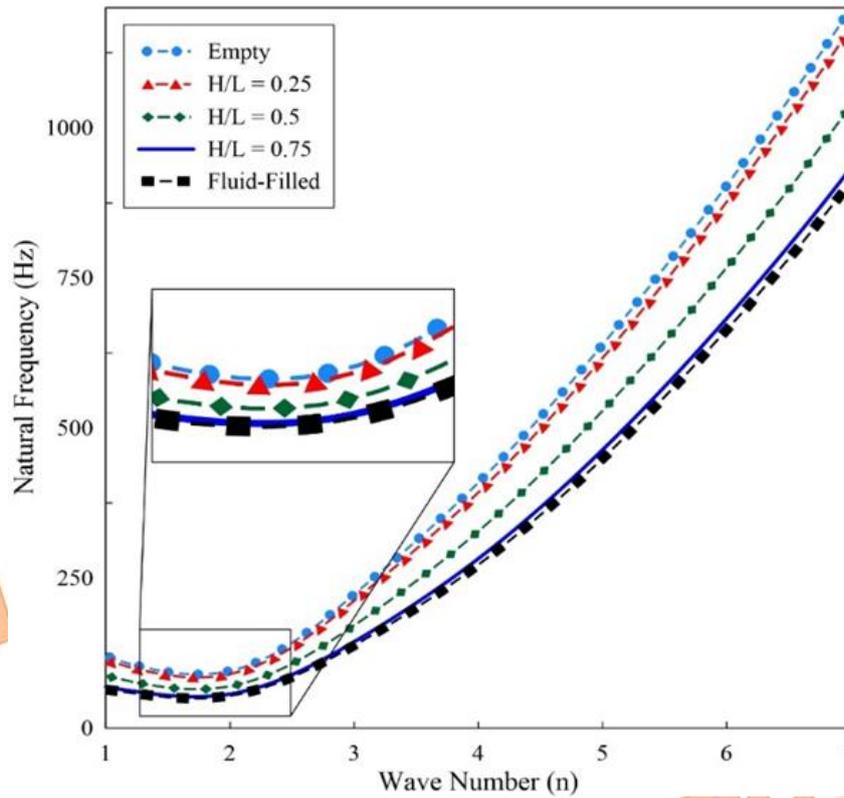
Fig. 10: Influence of Liquid Height on the Natural Frequency of a Cylindrical Shell (m=1)
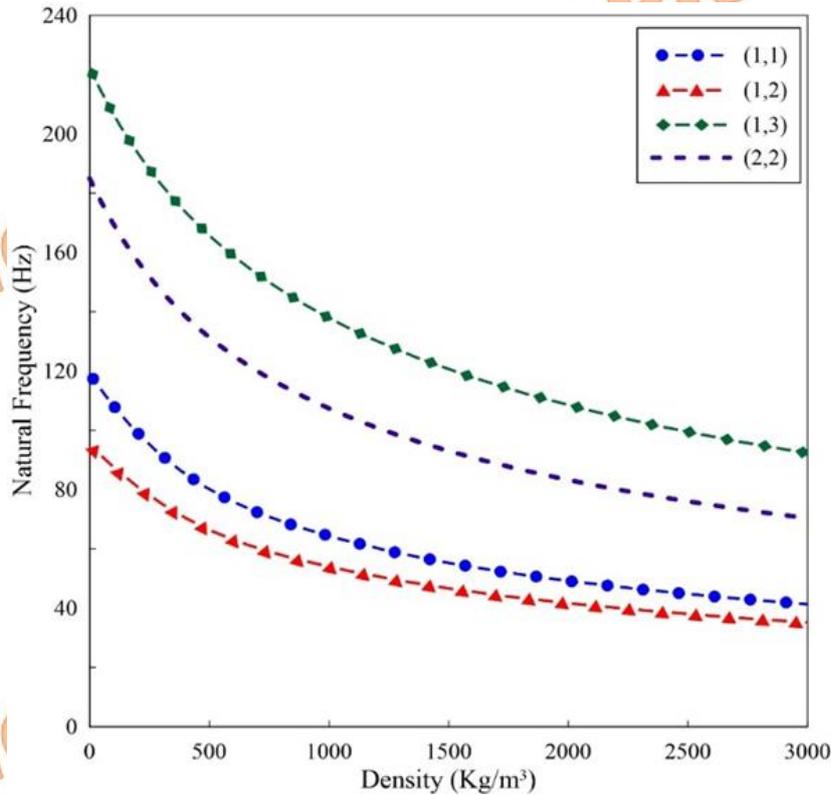

Fig. 11: Influence of Liquid Density on the Natural Frequency of a Liquid-Filled Shell

7. Conclusion

This article investigates the free vibration of a three-layer cylindrical shell with an auxetic core containing a liquid. The governing equations of this research were derived using modified high-order shear theories by applying Hamilton's principle. The weighted Galerkin residual method is used to solve the selected equations and obtain the natural frequencies. The results obtained from the theories used in this study agree with those obtained from other reference articles, as well as the output of the finite element software.

The impact of different adjustable parameters of the cylindrical shell and the auxetic core on the natural frequency was investigated, and the following results were obtained:

Among shells with different boundary conditions, those with both-ends clamped boundary conditions exhibit a higher natural frequency than shells with simple both-ends boundary conditions, assuming the thickness h remains constant for all length ratios.

As the L/R ratio increases, the natural frequency decreases due to reducing the stiffness-to-mass ratio in the system.

As the L/R ratio increases, the strength-to-mass ratio of the cylindrical shell grows. Consequently, the natural frequencies of the system also increase. However, when the L/R ratio reaches an optimal level, further increases in thickness will not significantly impact the natural frequencies.

In thin and moderately thick shells, the system's natural frequency increases with the increase of the ratio $\frac{h_c}{h}$ while keeping h constant.

The optimal value for the ratio $\frac{h_c}{h}$ is equal to 0.7 to 0.8. Within this interval, the natural frequencies of the system will reach their maximum values and subsequently decrease.

The change in the angle of the unit cell of the auxetic core can impact the system's natural frequencies. In thin and relatively thick shells, using smaller angles for the unit cell leads to an increase in the system's natural frequency.

The presence of liquid inside the cylindrical shell affects the system's natural frequencies. As the shell gradually fills with liquid, its mass increases, resulting in a decrease in the natural frequency values. Furthermore, as the liquid density increases, its impact on the system's natural frequency diminishes.

The above findings, based on the study's results, can assist the designers of structures with similar characteristics and serve as the foundation for their work. The use of cylindrical sandwich shells with an auxetic structure in their central layer can vary depending on the conditions and the designers' opinions. Common examples include the construction of trusses, metal frameworks for structures, and various applications in the medical engineering industry and the oil and gas industry.

Nomenclature

A Area, m2
E Modulus of Elasticity, N/m2
$f_1(z)$ considered for different theories
$f_2(z)$ considered for different theories
G shear modulus, N/m2
h total thickness of shell
H height of liquid

L Length of shell
R radius of shell
T kinetic energy
T_f kinetic energy of fluid
t Time, s
u_0 Longitudinal displacement of middle plane
u_1 Longitudinal displacement
u_2 circumferential displacement
u_3 transverse displacement
U strain energy
v_0 circumferential displacement of middle plane
w_0 transverse displacement of middle plane
x, θ, z Cylindrical coordinate parameters
ρ Density, kg/m3
ν Poisson's ratio
δ the variation of function
φ_1 represent the rotation of the middle plane around the θ axes
φ_2 represent the rotation of the middle plane around the x axes

Conflicts of Interest

The author declares that there is no conflict of interest regarding the publication of this article.

AppendixA

$$N_{xx} = \frac{A_1}{R}\left(\frac{\partial v_0}{\partial \theta} + w_0\right) + \frac{A_2}{R}\frac{\partial \phi_2}{\partial \theta}$$
$$+ \frac{A_3}{R^2}\left(\frac{\partial^2 w_0}{\partial \theta^2} - \frac{\partial v_0}{\partial \theta}\right)$$
$$+ B_1\frac{\partial u_0}{\partial x} + B_2\frac{\partial \phi_1}{\partial x} \qquad \text{(A-1)}$$
$$+ B_3\frac{\partial^2 w_0}{\partial x^2}$$

$$N_{x\theta} = C_1\frac{\partial v_0}{\partial x} + C_2\frac{\partial \phi_2}{\partial x}$$
$$+ \frac{C_3}{R}\left(2\frac{\partial^2 w_0}{\partial x\partial \theta} - \frac{\partial v_0}{\partial x}\right) \qquad \text{(A-2)}$$
$$+ \frac{C_1}{R}\frac{\partial u_0}{\partial \theta} + \frac{C_2}{R}\frac{\partial \phi_1}{\partial \theta}$$

$$N_{\theta\theta} = \frac{F_1}{R}\left(\frac{\partial v_0}{\partial \theta} + w_0\right) + \frac{F_2}{R}\frac{\partial \phi_2}{\partial \theta}$$
$$+ \frac{F_3}{R^2}\left(\frac{\partial^2 w_0}{\partial \theta^2} - \frac{\partial v_0}{\partial \theta}\right)$$
$$+ A_1\frac{\partial u_0}{\partial x} + A_2\frac{\partial \phi_1}{\partial x} \qquad \text{(A-3)}$$
$$+ A_3\frac{\partial^2 w_0}{\partial x^2}$$

$$S_{xx} = \frac{A_3}{R}\left(\frac{\partial v_0}{\partial \theta} + w_0\right) + \frac{A_4}{R}\frac{\partial \phi_2}{\partial \theta}$$
$$+ \frac{A_5}{R^2}\left(\frac{\partial^2 w_0}{\partial \theta^2} - \frac{\partial v_0}{\partial \theta}\right)$$
$$+ B_3\frac{\partial u_0}{\partial x} + B_4\frac{\partial \phi_1}{\partial x} \qquad \text{(A-4)}$$
$$+ B_5\frac{\partial^2 w_0}{\partial x^2}$$

$$S_{\theta\theta} = \frac{F_3}{R}\left(\frac{\partial v_0}{\partial \theta} + w_0\right) + \frac{F_4}{R}\frac{\partial \phi_2}{\partial \theta}$$
$$+ \frac{F_5}{R^2}\left(\frac{\partial^2 w_0}{\partial \theta^2} - \frac{\partial v_0}{\partial \theta}\right)$$
$$+ A_3\frac{\partial u_0}{\partial x} + A_4\frac{\partial \phi_1}{\partial x} \qquad \text{(A-5)}$$
$$+ A_5\frac{\partial^2 w_0}{\partial x^2}$$

$$S_{x\theta} = C_3\frac{\partial v_0}{\partial x} + C_4\frac{\partial \phi_2}{\partial x}$$
$$+ \frac{C_5}{R}\left(2\frac{\partial^2 w_0}{\partial x\partial \theta} - \frac{\partial v_0}{\partial x}\right) \qquad \text{(A-6)}$$
$$+ \frac{C_3}{R}\frac{\partial u_0}{\partial \theta} + \frac{C_4}{R}\frac{\partial \phi_1}{\partial \theta}$$

$$P_{xx} = \frac{A_2}{R}\left(\frac{\partial v_0}{\partial \theta} + w_0\right) + \frac{A_6}{R}\frac{\partial \phi_2}{\partial \theta}$$
$$+ \frac{A_4}{R^2}\left(\frac{\partial^2 w_0}{\partial \theta^2} - \frac{\partial v_0}{\partial \theta}\right)$$
$$+ B_2\frac{\partial u_0}{\partial x} + B_6\frac{\partial \phi_1}{\partial x} \qquad \text{(A-7)}$$
$$+ B_4\frac{\partial^2 w_0}{\partial x^2}$$

$$P_{\theta\theta} = \frac{F_2}{R}\left(\frac{\partial v_0}{\partial \theta} + w_0\right) + \frac{F_6}{R}\frac{\partial \phi_2}{\partial \theta}$$
$$+ \frac{F_4}{R^2}\left(\frac{\partial^2 w_0}{\partial \theta^2} - \frac{\partial v_0}{\partial \theta}\right)$$
$$+ A_2\frac{\partial u_0}{\partial x} + A_6\frac{\partial \phi_1}{\partial x} \qquad \text{(A-8)}$$
$$+ A_4\frac{\partial^2 w_0}{\partial x^2}$$

$$P_{x\theta} = C_2\frac{\partial v_0}{\partial x} + C_6\frac{\partial \phi_2}{\partial x}$$
$$+ \frac{C_4}{R}\left(2\frac{\partial^2 w_0}{\partial x\partial \theta} - \frac{\partial v_0}{\partial x}\right) \qquad \text{(A-9)}$$
$$+ \frac{C_2}{R}\frac{\partial u_0}{\partial \theta} + \frac{C_6}{R}\frac{\partial \phi_1}{\partial \theta}$$

$$Q_{xz} = E_6\phi_1 + (E_3 + E_4)\frac{\partial w_0}{\partial x} \qquad \text{(A-10)}$$

$$Q_{\theta z} = \frac{(D_3 + D_4)}{R}\left(\frac{\partial w_0}{\partial \theta} - v_0\right) + D_6\phi_2 \qquad \text{(A-11)}$$

$$T_{xz} = (E_3 + E_4)\phi_1 + (E_1 + 2E_2 + E_5)\frac{\partial w_0}{\partial x} \qquad \text{(A-12)}$$

$$T_{\theta z} = (D_3 + D_4)\phi_2$$
$$+ \frac{(D_1 + 2D_2 + D_5)}{R}\left(\frac{\partial w_0}{\partial \theta}\right. \qquad \text{(A-13)}$$
$$\left. - v_0\right)$$

Coefficients A_i, B_i, C_i, D_i, E_i and F_i where ($1 \leq i \leq 6$) in relations (A-1) to (A-13) are defined as relations (A-14) to (A-19).

$$\{A_1, A_2, A_3, A_4, A_5, A_6\}$$
$$= \sum_{k=1}^{3}\int_{z_{k-1}}^{z_k} Q_{12}^{(k)}\{1, f_2, f_1, f_1 f_2, f_1^2, f_2^2\}\, dz \qquad \text{(A-14)}$$

$$\{B_1, B_2, B_3, B_4, B_5, B_6\}$$
$$= \sum_{k=1}^{3}\int_{z_{k-1}}^{z_k} Q_{11}^{(k)}\{1, f_2, f_1, f_1 f_2, f_1^2, f_2^2\}\, dz \qquad \text{(A-15)}$$

$$\{C_1, C_2, C_3, C_4, C_5, C_6\}$$
$$= \sum_{k=1}^{3}\int_{z_{k-1}}^{z_k} Q_{66}^{(k)}\{1, f_2, f_1, f_1 f_2, f_1^2, f_2^2\}\, dz \qquad \text{(A-16)}$$

$$\{D_1, D_2, D_3, D_4, D_5, D_6\} = \sum_{k=1}^{3}\int_{z_{k-1}}^{z_k} Q_{44}^{(k)}A\, dz \qquad \text{(A-17)}$$
where $A = \left\{1, \frac{\partial f_1}{\partial z}, \frac{\partial f_2}{\partial z}, \frac{\partial f_1}{\partial z}\frac{\partial f_2}{\partial z}, \left(\frac{\partial f_1}{\partial z}\right)^2, \left(\frac{\partial f_2}{\partial z}\right)^2\right\}$

$$\{E_1, E_2, E_3, E_4, E_5, E_6\} = \sum_{k=1}^{3}\int_{z_{k-1}}^{z_k} Q_{55}^{(k)}A\, dz \qquad \text{(A-18)}$$
where $A = \left\{1, \frac{\partial f_1}{\partial z}, \frac{\partial f_2}{\partial z}, \frac{\partial f_1}{\partial z}\frac{\partial f_2}{\partial z}, \left(\frac{\partial f_1}{\partial z}\right)^2, \left(\frac{\partial f_2}{\partial z}\right)^2\right\}$

$$\{F_1, F_2, F_3, F_4, F_5, F_6\}$$
$$= \sum_{k=1}^{3}\int_{z_{k-1}}^{z_k} Q_{22}^{(k)}\{1, f_2, f_1, f_1 f_2, f_1^2, f_2^2\}\, dz \qquad \text{(A-19)}$$

By substituting the relationships related to forces and moments (A-1) to (A-13) into the governing equations expressed in terms of Eq. 16 to Eq. 20, it is possible to obtain the governing equations expressed in terms of displacement components, which are by relations (A-20) to (A-24).

$$\delta u_0: \frac{A_1}{R}\left(\frac{\partial^2 v_0}{\partial x\partial \theta} + \frac{\partial w_0}{\partial x}\right) + \frac{A_2}{R}\frac{\partial^2 \phi_2}{\partial x\partial \theta}$$
$$+ \frac{A_3}{R^2}\left(\frac{\partial^3 w_0}{\partial x\partial \theta^2} - \frac{\partial^2 v_0}{\partial x\partial \theta}\right)$$
$$+ B_1\frac{\partial^2 u_0}{\partial x^2} + B_2\frac{\partial^2 \phi_1}{\partial x^2}$$
$$+ B_3\frac{\partial^3 w_0}{\partial x^3}$$
$$+ \frac{1}{R}\left(C_1\frac{\partial^2 v_0}{\partial x\partial \theta} + C_2\frac{\partial^2 \phi_2}{\partial x\partial \theta}\right.$$
$$+ \frac{C_3}{R}\left(2\frac{\partial^3 w_0}{\partial x\partial \theta^2} - \frac{\partial^2 v_0}{\partial x\partial \theta}\right) \qquad \text{(A-20)}$$
$$\left. + \frac{C_1}{R}\frac{\partial^2 u_0}{\partial \theta^2} + \frac{C_2}{R}\frac{\partial^2 \phi_1}{\partial \theta^2}\right)$$
$$= I_0\frac{\partial^2 u_0}{\partial t^2} + I_1\frac{\partial^3 w_0}{\partial x\partial t^2}$$
$$+ I_3\frac{\partial^2 \phi_1}{\partial t^2}$$

19

$$\delta v_0: \frac{1}{R}\left(\frac{F_1}{R}\left(\frac{\partial^2 v_0}{\partial\theta^2}+\frac{\partial w_0}{\partial\theta}\right)+\frac{F_2}{R}\frac{\partial^2\phi_2}{\partial\theta^2}+\frac{F_3}{R^2}\left(\frac{\partial^3 w_0}{\partial\theta^3}-\frac{\partial^2 v_0}{\partial\theta^2}\right)+A_1\frac{\partial^2 u_0}{\partial x\partial\theta}+A_2\frac{\partial^2\phi_1}{\partial x\partial\theta}+A_3\frac{\partial^3 w_0}{\partial x^2\partial\theta}\right)$$
$$-\frac{1}{R^2}\left(\frac{F_3}{R}\left(\frac{\partial^2 v_0}{\partial\theta^2}+\frac{\partial w_0}{\partial\theta}\right)+\frac{F_4}{R}\frac{\partial^2\phi_2}{\partial\theta^2}+\frac{F_5}{R^2}\left(\frac{\partial^3 w_0}{\partial\theta^3}-\frac{\partial^2 v_0}{\partial\theta^2}\right)+A_3\frac{\partial^2 u_0}{\partial x\partial\theta}+A_4\frac{\partial^2\phi_1}{\partial x\partial\theta}+A_5\frac{\partial^3 w_0}{\partial x^2\partial\theta}\right)$$
$$+C_1\frac{\partial^2 v_0}{\partial x^2}+C_2\frac{\partial^2\phi_2}{\partial x^2}+\frac{C_3}{R}\left(2\frac{\partial^3 w_0}{\partial x^2\partial\theta}-\frac{\partial^2 v_0}{\partial x^2}\right)+\frac{C_1}{R}\frac{\partial^2 u_0}{\partial x\partial\theta}+\frac{C_2}{R}\frac{\partial^2\phi_1}{\partial x\partial\theta}$$
$$-\frac{1}{R}\left(C_3\frac{\partial^2 v_0}{\partial x^2}+C_4\frac{\partial^2\phi_2}{\partial x^2}+\frac{C_5}{R}\left(2\frac{\partial^3 w_0}{\partial x^2\partial\theta}-\frac{\partial^2 v_0}{\partial x^2}\right)+\frac{C_3}{R}\frac{\partial^2 u_0}{\partial x\partial\theta}+\frac{C_4}{R}\frac{\partial^2\phi_1}{\partial x\partial\theta}\right)$$
$$+\frac{1}{R}\left((D_3+D_4)\phi_2+\frac{(D_1+2D_2+D_5)}{R}\left(\frac{\partial w_0}{\partial\theta}-v_0\right)\right)$$
$$=\left(I_0-\frac{2I_1}{R}+\frac{I_2}{R^2}\right)\frac{\partial^2 v_0}{\partial t^2}+\left(\frac{I_1}{R}-\frac{I_2}{R^2}\right)\frac{\partial^3 w_0}{\partial\theta\partial t^2}+\left(I_3-\frac{I_5}{R}\right)\frac{\partial^2\phi_2}{\partial t^2} \qquad \text{(A-21)}$$

$$\delta w_0:(E_3+E_4)\frac{\partial\phi_1}{\partial x}+(E_1+2E_2+E_5)\frac{\partial^2 w_0}{\partial x^2}+\frac{1}{R}\left((D_3+D_4)\frac{\partial\phi_2}{\partial\theta}+\frac{(D_1+2D_2+D_5)}{R}\left(\frac{\partial^2 w_0}{\partial\theta^2}-\frac{\partial v_0}{\partial\theta}\right)\right)$$
$$-\frac{A_3}{R}\left(\frac{\partial^3 v_0}{\partial x^2\partial\theta}+\frac{\partial^2 w_0}{\partial x^2}\right)-\frac{A_4}{R}\frac{\partial^3\phi_2}{\partial x^2\partial\theta}-\frac{A_5}{R^2}\left(\frac{\partial^4 w_0}{\partial x^2\partial\theta^2}-\frac{\partial^3 v_0}{\partial x^2\partial\theta}\right)-B_3\frac{\partial^3 u_0}{\partial x^3}-B_4\frac{\partial^3\phi_1}{\partial x^3}$$
$$-B_5\frac{\partial^4 w_0}{\partial x^4}$$
$$-\frac{1}{R^2}\left(\frac{F_3}{R}\left(\frac{\partial^3 v_0}{\partial\theta^3}+\frac{\partial^2 w_0}{\partial\theta^2}\right)+\frac{F_4}{R}\frac{\partial^3\phi_2}{\partial\theta^3}+\frac{F_5}{R^2}\left(\frac{\partial^4 w_0}{\partial\theta^4}-\frac{\partial^3 v_0}{\partial\theta^3}\right)+A_3\frac{\partial u_0}{\partial x}+A_4\frac{\partial^3\phi_1}{\partial x\partial\theta^2}\right.$$
$$\left.+A_5\frac{\partial^4 w_0}{\partial x^2\partial\theta^2}\right) \qquad \text{(A-22)}$$
$$-\frac{1}{R}\left(\frac{F_1}{R}\left(\frac{\partial v_0}{\partial\theta}+w_0\right)+\frac{F_2}{R}\frac{\partial\phi_2}{\partial\theta}+\frac{F_3}{R^2}\left(\frac{\partial^2 w_0}{\partial\theta^2}-\frac{\partial v_0}{\partial\theta}\right)+A_1\frac{\partial u_0}{\partial x}+A_2\frac{\partial\phi_1}{\partial x}+A_3\frac{\partial^2 w_0}{\partial x^2}\right)$$
$$-\frac{2}{R}\left(C_3\frac{\partial^3 v_0}{\partial x^2\partial\theta}+C_4\frac{\partial^3\phi_2}{\partial x^2\partial\theta}+\frac{C_5}{R}\left(2\frac{\partial^4 w_0}{\partial x^2\partial\theta^2}-\frac{\partial^3 v_0}{\partial x^2\partial\theta}\right)+\frac{C_3}{R}\frac{\partial^3 u_0}{\partial x\partial\theta^2}+\frac{C_4}{R}\frac{\partial^3\phi_1}{\partial x\partial\theta^2}\right)$$
$$=I_0\frac{\partial^2 w_0}{\partial t^2}-I_1\frac{\partial^3 u_0}{\partial x\partial t^2}-(I_2+I_5)\frac{\partial^4 w_0}{\partial x^2\partial t^2}-I_5\frac{\partial^3\phi_1}{\partial x\partial t^2}-\left(\frac{I_1}{R}-\frac{I_2}{R^2}\right)\frac{\partial^3 v_0}{\partial\theta\partial t^2}-\frac{I_2}{R^2}\frac{\partial^4 w_0}{\partial\theta^2\partial t^2}$$
$$-\frac{I_5}{R}\frac{\partial^3\phi_2}{\partial\theta\partial t^2}$$

$$\delta\phi_1=\frac{A_2}{R}\left(\frac{\partial^2 v_0}{\partial x\partial\theta}+\frac{\partial w_0}{\partial x}\right)+\frac{A_6}{R}\frac{\partial^2\phi_2}{\partial x\partial\theta}+\frac{A_4}{R^2}\left(\frac{\partial^3 w_0}{\partial x\partial\theta^2}-\frac{\partial^2 v_0}{\partial x\partial\theta}\right)+B_2\frac{\partial^2 u_0}{\partial x^2}+B_6\frac{\partial^2\phi_1}{\partial x^2}+B_4\frac{\partial^3 w_0}{\partial x^3}$$
$$+\frac{1}{R}\left(C_2\frac{\partial^2 v_0}{\partial x\partial\theta}+C_6\frac{\partial^2\phi_2}{\partial x\partial\theta}+\frac{C_4}{R}\left(2\frac{\partial^3 w_0}{\partial x\partial\theta^2}-\frac{\partial^2 v_0}{\partial x\partial\theta}\right)+\frac{C_2}{R}\frac{\partial^2 u_0}{\partial\theta^2}+\frac{C_6}{R}\frac{\partial^2\phi_1}{\partial\theta^2}\right)-E_6\phi_1 \qquad \text{(A-23)}$$
$$-(E_3+E_4)\frac{\partial w_0}{\partial x}=I_3\frac{\partial^2 u_0}{\partial t^2}+I_4\frac{\partial^2\phi_1}{\partial t^2}$$

$$\delta\phi_2=C_2C_2\frac{\partial^2 v_0}{\partial x^2}+C_6\frac{\partial^2\phi_2}{\partial x^2}+\frac{C_4}{R}\left(2\frac{\partial^3 w_0}{\partial x^2\partial\theta}-\frac{\partial^2 v_0}{\partial x^2}\right)+\frac{C_2}{R}\frac{\partial^2 u_0}{\partial x\partial\theta}+\frac{C_6}{R}\frac{\partial^2\phi_1}{\partial x\partial\theta}$$
$$+\frac{1}{R}\left(\frac{F_2}{R}\left(\frac{\partial^2 v_0}{\partial\theta^2}+\frac{\partial w_0}{\partial\theta}\right)+\frac{F_6}{R}\frac{\partial^2\phi_2}{\partial\theta^2}+\frac{F_4}{R^2}\left(\frac{\partial^3 w_0}{\partial\theta^3}-\frac{\partial^2 v_0}{\partial\theta^2}\right)+A_2\frac{\partial^2 u_0}{\partial x\partial\theta}+A_6\frac{\partial^2\phi_1}{\partial x\partial\theta}+A_4\frac{\partial^3 w_0}{\partial x^2\partial\theta}\right) \qquad \text{(A-24)}$$
$$-\frac{(D_3+D_4)}{R}\left(\frac{\partial w_0}{\partial\theta}-v_0\right)-D_6\phi_2=\left(I_3-\frac{I_5}{R}\right)\frac{\partial^2 v_0}{\partial t^2}+\frac{I_5}{R}\frac{\partial^3 w_0}{\partial\theta\partial t^2}+I_4\frac{\partial^2\phi_2}{\partial t^2}$$

References

[1] Luo, C., Han, C.Z., Zhang, X.Y., Zhang, X.G., Ren, X. & Xie, Y.M., 2021. Design, manufacturing and applications of auxetic tubular structures: A review. *Thin-Walled Structures, 163*, pp.107682.

[2] Gill, H.S., 2021. Mechanical and structure properties of cellular auxetic materials. *Materials Today: Proceedings, 37*, pp.3320-3323.

[3] Joseph, A., Mahesh, V. & Harursampath, D., 2021. On the application of additive manufacturing methods for auxetic structures: A review. *Advances in Manufacturing, 9* (3), pp.342-368.

[4] Nguyễn, H., Fangueiro, R., Ferreira, F. & Nguyễn, Q., 2023. Auxetic materials and structures for potential defense applications: An overview and recent developments. *Textile Research Journal, 93* (23-24), pp.5268-5306.

[5] Salehi, M., Bakhtiarinezhad, F. & Besharati, A., 2008. Time-domain analysis of sandwich shells with passive constrained viscoelastic layers.

[6] Ranjbar, M., Boldrin, L., Scarpa, F., Neild, S. & Patsias, S., 2016. Vibroacoustic optimization of anti-tetrachiral and auxetic hexagonal sandwich panels with gradient geometry. *Smart Materials and Structures, 25* (5), pp.054012.

[7] Mazloomi, M.S., Ranjbar, M., Boldrin, L., Scarpa, F., Patsias, S. & Ozada, N., 2018. Vibroacoustics of 2d gradient auxetic hexagonal honeycomb sandwich panels. *Composite Structures, 187*, pp.593-603.

[8] Hosseinkhani, A., Younesian, D. & Ranjbar, M., 2020. Vibro-acoustic analysis and topology optimization of anti-tetra chiral auxetic lattices driven by different colored noises. *International*

Journal of Structural Stability and Dynamics, 20 (11), pp.2050113.

[9] Hosseinkhani, A., Younesian, D., Ranjbar, M. & Scarpa, F., 2021. Enhancement of the vibro-acoustic performance of anti-tetra-chiral auxetic sandwich panels using topologically optimized local resonators. *Applied Acoustics, 177*, pp.107930.

[10] Mazloomi, M.S. & Ranjbar, M., 2021. Hybrid design optimization of sandwich panels with gradient shape anti-tetrachiral auxetic core for vibroacoustic applications. *Transport in Porous Media*, pp.1-18.

[11] Pakrooyan, A., Yousefi, P., Khorshidi, K., Najafizadeh, M.M. & Nezamabadi, A., 2022. Free vibration analysis of an auxetic honeycomb sandwich plate placed at the wall of a fluid tank. *Ocean Engineering, 263*, pp.112353.

[12] Khorshidi, K., Rezaeisaray, M. & Karimi, M., 2022. Energy harvesting using vibrating honeycomb sandwich panels with auxetic core and carbon nanotube-reinforced face sheets. *International Journal of Solids and Structures, 256*, pp.111988.

[13] Duc, N.D., Seung-Eock, K., Tuan, N.D., Tran, P. & Khoa, N.D., 2017. New approach to study nonlinear dynamic response and vibration of sandwich composite cylindrical panels with auxetic honeycomb core layer. *Aerospace Science and Technology, 70*, pp.396-404.

[14] Fu, T., Hu, X. & Yang, C., 2023. Impact response analysis of stiffened sandwich functionally graded porous materials doubly-curved shell with re-entrant honeycomb auxetic core. *Applied Mathematical Modelling, 124*, pp.553-575.

[15] Karimiasl, M. & Alibeigloo, A., 2022. Nonlinear free and forced vibration analysis of sandwich cylindrical panel with auxetic core and gplrc facing sheets in hygrothermal environment. *Thin-Walled Structures, 175*, pp.109164.

[16] Khorshidi, K., Savvafi, S. & Zobeid, S., 2024. Forced vibration of a three-layer cylindrical shell with an auxetic core containing fluid under the influence of shock load using high-order shear deformation theories. *Mechanic of Advanced and Smart Materials, 3* (4), pp.431-464.

[17] Khorshidi, K. & Karimi, M., 2019. Analytical modeling for vibrating piezoelectric nanoplates in interaction with inviscid fluid using various modified plate theories. *Ocean Engineering, 181*, pp.267-280.

[18] Sheng, G. & Wang, X., 2008. Thermomechanical vibration analysis of a functionally graded shell with flowing fluid. *European Journal of Mechanics-A/Solids, 27* (6), pp.1075-1087.

[19] Zhu, X., Zhang, J., Zhang, W. & Chen, J., 2019. Vibration frequencies and energies of an auxetic honeycomb sandwich plate. *Mechanics of Advanced Materials and Structures, 26* (23), pp.1951-1957.

[20] Mehdianfar, P., Shabani, Y. & Khorshidi, K., 2022. Natural frequency of sandwich beam structures with two dimensional functionally graded porous layers based on novel formulations. *International Journal of Engineering, 35* (11), pp.2092-2101.

[21] Kim, Y.-W., Lee, Y.-S. & Ko, S.-H., 2004. Coupled vibration of partially fluid-filled cylindrical shells with ring stiffeners. *Journal of Sound and Vibration, 276* (3-5), pp.869-897.

[22] Khorshidi, K., 2012. Effect of hydrostatic pressure and depth of fluid on the vibrating rectangular plates partially in contact with a fluid. *Applied Mechanics and Materials, 110*, pp.927-935.

[23] Kayran, A., 1990. *Free vibration analysis of laminated composite shells of revolution including transverse shear deformation*. University of Delaware.

[24] Khorshidi, K., Soltannia, B., Karimi, M. & Ghorbani, A., 2023. Nonlinear vibration of electro-rheological sandwich plates, coupled to quiescent fluid. *Ocean Engineering, 271*, pp.113730.

[25] Loy, C., Lam, K. & Shu, C., 1997. Analysis of cylindrical shells using generalized differential quadrature. *Shock and vibration, 4* (3), pp.193-198.

[26] Qu, Y., Hua, H. & Meng, G., 2013. A domain decomposition approach for vibration analysis of isotropic and composite cylindrical shells with arbitrary boundaries. *Composite Structures, 95*, pp.307-321.

[27] Khalili, S., Davar, A. & Fard, K.M., 2012. Free vibration analysis of homogeneous isotropic circular cylindrical shells based on a new three-dimensional refined higher-order theory. *International journal of Mechanical sciences, 56* (1), pp.1-25.

[28] Loy, C. & Lam, K., 1999. Vibration of thick cylindrical shells on the basis of three-dimensional theory of elasticity. *Journal of sound and Vibration, 226* (4), pp.719-737.

[29] Lakis, A.A. & Sinno, M., 1992. Free vibration of axisymmetric and beam-like cylindrical shells, partially filled with liquid. *International Journal for Numerical Methods in Engineering, 33* (2), pp.235-268.

[30] Amabili, M., Païdoussis, M.P. & Lakis, A.A., 1998. Vibrations of partially filled cylindrical tanks with ring-stiffeners and flexible bottom. *Journal of Sound and Vibration, 213* (2), pp.259-299.

[31] Niordson, F.I., 1953. *Vibrations of a cylindrical tube containing flowing fluid*. Lindståhl.